symmetry

MDPI

Review

Applications of Substrate Materials for Interdigital Transducers (IDTs): A Review

Ziping Wang [1,*], Haitao Zhang [1], Chengxu Wang [1], Xilin Wang [2], Alfredo Güemes [1,3] and Nataša R. Trišović [4]

[1] School of Low-Altitude Technology, Jiangsu University, Zhenjiang 212013, China; 2212423007@stmail.ujs.edu.cn (H.Z.); 2212523021@stmail.ujs.edu.cn (C.W.); alfredo.guemes@upm.es (A.G.)
[2] Institute of Ocean Engineering, Shenzhen International Graduate School, Tsinghua University, Shenzhen 518055, China; wang.xilin@sz.tsinghua.edu.cn
[3] Department of Aeronautics, Polytechnic University of Madrid, 28040 Madrid, Spain
[4] Faculty of Mechanical Engineering, University of Belgrade, Kraljice Marije 16, 11120 Belgrade, Serbia; ntrisovic@mas.bg.ac.rs
* Correspondence: wzpxx2004@126.com

Abstract

Structural health monitoring (SHM) based on ultrasonic-guided waves has been widely investigated for aerospace, transportation, marine engineering, petrochemical equipment and large-scale civil infrastructure. As the core component for guided-wave excitation and signal reception, the transducer directly affects electromechanical conversion efficiency, modal selectivity and service stability. Interdigital transducers (IDTs) are characterized by a lightweight structure, designable wavelength, tunable operating frequency and good array compatibility, and therefore show considerable potential for curved structures, composite components and large-area online monitoring. The periodically repeated interdigital electrode pattern represents a basic form of structural symmetry in IDTs, providing the geometric basis for wavelength matching and frequency-selective response, while substrate properties govern the electromechanical conversion efficiency and stability of the device. This review focuses on the research progress of substrate materials for flexible IDTs. The material characteristics and application status of inorganic piezoelectric materials, piezoelectric polymers, piezoelectric composites and heterogeneous integrated substrates are summarized. The differences among typical substrate systems are compared in terms of electromechanical coupling, flexible conformability, thermal stability, acoustic loss and integration process. Recent applications of IDTs in guided-wave damage detection, flexible sensing, high-temperature monitoring and on-chip acoustic devices are also discussed. The main challenges and future directions of IDT substrate materials are analyzed to provide guidance for material selection, device design and SHM applications.

Keywords: flexible interdigital transducer; substrate material; ultrasonic-guided wave; structural health monitoring; piezoelectric thin film; flexible sensing

Check for updates

Academic Editor: Vasilis K. Oikonomou

Received: 12 July 2026
Revised: 13 August 2026
Accepted: 21 August 2026
Published: 24 August 2026

1. Introduction

Critical engineering structures in the petrochemical industry, aerospace, marine engineering and large-scale infrastructure are continuously affected by alternating loads, changes in temperature and humidity, corrosive media, material aging and manufacturing defects during long-term service. Cracks, debonding, delamination, corrosion thinning and fatigue damage may gradually accumulate in such structures [1–6]. If these early defects cannot be identified in time, their continuous growth may reduce the load-bearing capacity of structures and even lead to severe safety accidents [4,7–9]. Therefore, structural health monitoring (SHM) technology is of great significance for safe operation, service life extension and maintenance decision-making of complex engineering structures [10–31]. Representative engineering scenarios for IDT-based monitoring are summarized in Figure 1.

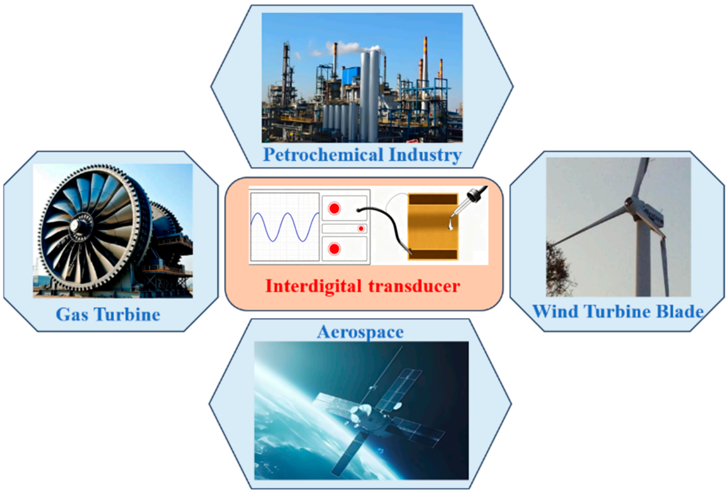

Figure 1. Typical application scenarios of interdigital transducers in the petrochemical industry, aerospace, gas turbines and wind turbine blades.

Conventional nondestructive testing methods, such as visual inspection, radiographic testing, magnetic particle testing and conventional ultrasonic testing, have been widely used for local defect identification [32–38]. However, for large-scale structures, complex configurations or harsh service environments, these methods still suffer from limited inspection coverage, strong dependence on manual operation, relatively low efficiency and difficulty in online monitoring [39–43]. In contrast, SHM integrates sensors, actuators, data acquisition and analysis systems into target structures, enabling continuous perception of structural states and early damage warning, and providing an effective means for early defect recognition and remaining-life assessment [44–52].

Among various SHM techniques, ultrasonic-guided waves have attracted extensive attention because they can propagate over long distances with relatively low attenuation, are sensitive to local defects such as cracks and delamination, and can cover large inspection areas [52–65]. Lamb waves can propagate in plate-like structures over long distances. By selecting the frequency, mode and propagation path, they can be used for different types of damage in aerospace composites, ship structures, bridge components and storage or transportation pipelines [66–73]. It should be noted that guided-wave inspection performance depends not only on signal processing algorithms but also strongly on transducer excitation efficiency, receiving sensitivity, modal selectivity and coupling condition with the host structure.

An interdigital transducer (IDT) is a functional device that realizes mutual conversion between electrical signals and elastic waves through periodic interdigital electrodes [74–76]. Compared with conventional bulk piezoelectric transducers, IDTs are thin, lightweight, designable in center frequency and excitation wavelength, easy to form into arrays and suitable for large-area deployment [76,77]. By adjusting geometric parameters such as electrode period, finger spacing, finger width and aperture, IDTs can control guided-wave propagation direction, center frequency and excitation mode, thereby providing a hardware basis for directional excitation, multipoint monitoring and regional damage imaging in complex structures [78–80]. The periodically repeated electrode fingers can therefore be regarded as a form of structural symmetry, and this spatial regularity provides the basis for wavelength matching, coherent wave superposition, and frequency-selective excitation.

The performance of an IDT is not determined only by the electrode structure. The substrate material is also a key factor influencing device performance [81,82]. Piezoelectricity, dielectric properties, thermal stability, flexibility and interfacial integrity of the substrate affect electromechanical coupling efficiency, guided-wave propagation loss, frequency stability, environmental adaptability and long-term service performance [83]. From this perspective, substrate selection is also important for maintaining the regular electrode–substrate configuration and ensuring a stable acoustoelectric response under bending, temperature variation, and long-term service conditions. A systematic review of substrate materials for IDTs is therefore necessary. Different substrates show distinct advantages and limitations in electromechanical coupling, guided-wave excitation, flexible conformability and temperature resistance. Meanwhile, SHM, wearable sensing, high-temperature monitoring and on-chip acoustic devices impose different requirements on IDT substrate materials [84]. This review focuses on the progress and applications of flexible IDT substrate materials and provides references for material selection, device optimization and engineering design.

2. Working Principle and Frequency Response of IDTs

2.1. Basic Structure and Electromechanical Conversion Mechanism

When an IDT works as an actuator, an alternating voltage applied to adjacent interdigital electrodes generates a periodic electric field. Under the inverse piezoelectric effect, periodic mechanical deformation is produced in the piezoelectric material and elastic waves are radiated [85–96]. When an IDT works as a receiver, external elastic waves induce strain variation in the piezoelectric substrate, and an electrical signal is generated between electrodes through the direct piezoelectric effect [97–102]. Thus, an IDT is essentially a bidirectional energy converter based on the direct and inverse piezoelectric effects.

The frequency selectivity of an IDT originates from the periodic spatial distribution of interdigital electrodes. Only when the electrode period satisfies the phase-matching condition with the target acoustic wavelength can waves excited by individual electrodes be constructively superimposed and produce a high response. When the excitation frequency deviates from this condition, phase cancelation occurs and the response amplitude decreases.

2.2. Frequency Response Relationship

The center frequency of an IDT is mainly determined by the acoustic velocity and electrode period. Let the wavelength be λ_0, the acoustic velocity be v_s, the acoustic propagation period be T and the center frequency be f_0. The basic relationship is

$$\lambda_0 = v_s T = \frac{v_s}{f_0} \tag{1}$$

For a conventional uniformly spaced IDT, if the width of one electrode is a and the spacing between adjacent electrodes is b, the pitch can be expressed as

$$p = a + b \tag{2}$$

Because adjacent electrodes with the same polarity correspond to one complete spatial period, the excited wavelength is usually

$$\lambda_0 = 2p = 2(a + b) \tag{3}$$

Accordingly, the acoustic synchronous frequency or center frequency is

$$f_c = \frac{v_s}{\lambda_0} = \frac{v_s}{2(a+b)} \tag{4}$$

For surface acoustic wave devices, v_s is generally the surface acoustic wave velocity of the piezoelectric substrate. For Lamb-wave IDTs, the phase velocity c_p of the target mode at the corresponding frequency should be used. Because Lamb waves are dispersive and their velocity varies with the frequency–thickness product, the IDT design should be combined with dispersion curves and satisfy

$$\lambda = \frac{c_p}{f} \tag{5}$$

Therefore, the structural design of an IDT is essentially a matching problem between the electrode period and the target acoustic wavelength. A smaller pitch corresponds to a higher center frequency, whereas a larger pitch corresponds to a lower center frequency. The corresponding geometric parameters are illustrated in Figure 2.

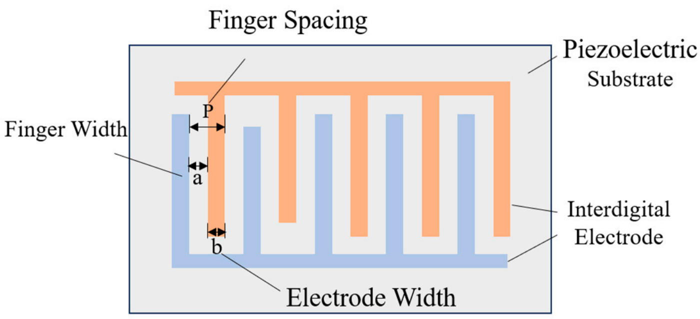

Figure 2. Structural schematic of an interdigital transducer, showing finger spacing, finger width, electrode width, interdigital electrode and piezoelectric substrate.

2.3. Frequency Response Analysis Based on the Delta-Function Model

To describe the frequency response of an IDT, the delta-function model can be used for equivalent analysis. In this model, each electrode finger is treated as a discrete acoustic source, and the entire IDT is regarded as the superposition of periodically distributed delta-function sources [103–106].

Assume that the IDT has N finger pairs. For the n-th electrode, the acoustic amplitude is a_n, the polarity factor is s_n and the time delay from the first electrode to the n-th electrode is t_n. The impulse response can be expressed as

$$h(t) = \sum_{n=1}^{N} s_n a_n \delta(t - t_n) \tag{6}$$

After Fourier transformation, the frequency response function of the IDT is

$$H(\omega) = \int_{-\infty}^{+\infty} h(t)^{e-j\omega t} dt = \sum_{n=1}^{2N} s_n a_n e^{-j\omega t_n} \tag{7}$$

This expression indicates that the frequency response of an IDT results from the coherent superposition of equivalent acoustic sources in the frequency domain. When the excitation frequency satisfies the phase-matching condition, the sources are superimposed in phase and the response reaches its maximum. When the frequency deviates from the center frequency, phase differences among the sources reduce the response amplitude.

For a uniform periodic IDT with a metallization ratio of η = 0.5, the amplitudes of the electrodes can be considered approximately equal, and the response can be written in a form containing the familiar array factor:

$$H(\omega) = a_0 \frac{sin(2N\frac{\theta}{2})}{sin(\frac{\theta}{2})} e^{j\varphi} \quad (8)$$

where θ is the phase difference between adjacent equivalent sources and φ is a phase term. The frequency response therefore has clear main-lobe and side-lobe characteristics. When the frequency is close to the center frequency, the main-lobe amplitude is the highest; as the frequency deviates from the center frequency, the response gradually weakens.

The number of finger pairs N strongly affects the response. As N increases, more sources participate in coherent superposition, the main-lobe amplitude increases and frequency selectivity is enhanced; however, the main-lobe width decreases and the bandwidth becomes narrower. Thus, IDTs with many finger pairs are suitable for narrow-band and highly selective excitation, while IDTs with fewer finger pairs provide broader bandwidth but relatively lower output amplitude and modal selectivity. The normalized responses for representative finger-pair numbers are compared in Figure 3.

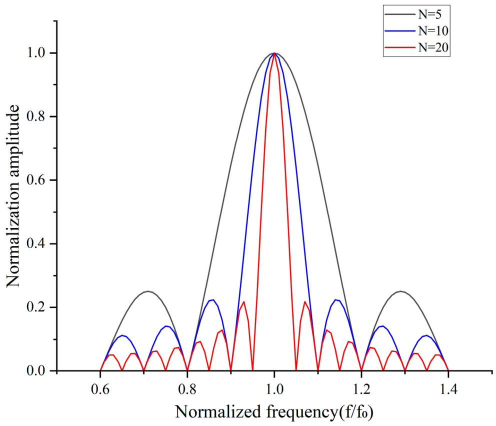

Figure 3. Normalized frequency response of a uniform IDT for different numbers of finger pairs N, illustrating the increase in frequency selectivity and the reduction in main-lobe bandwidth as N increases.

In summary, the frequency response of an IDT is jointly determined by electrode geometry, target acoustic mode and substrate properties. The interdigital structure provides frequency and wavelength selectivity, while the acoustic velocity, piezoelectric properties, dielectric loss and mechanical characteristics of the substrate further affect practical conversion efficiency, propagation loss and response stability. Therefore, structural parameter optimization should be coordinated with substrate material selection.

3. Development Status of IDT Substrate Materials

An IDT generally consists of a piezoelectric substrate and a comb-like metal electrode pattern fabricated on its surface. Preparing high-performance piezoelectric substrates is one of the important directions for optimizing interdigital transducers [107–115]. By applying an alternating voltage to the interdigital electrodes, the direct and inverse piezoelectric effects are used to realize energy conversion between the electrical and mechanical domains, as well as conversion between acoustic waves and electrical signals. According to material type, piezoelectric substrates can be classified as inorganic piezoelectric materials, piezoelectric polymers and piezoelectric composites.

3.1. Inorganic Piezoelectric Substrates

Inorganic piezoelectric materials are among the earliest and most extensively studied substrate systems for IDTs [65,66,70]. They usually have a high piezoelectric response, low acoustic loss and good frequency stability, and are suitable for SAW devices, Lamb-wave resonators, ultrasonic transducers and SHM. However, they are generally stiff and brittle, which limits direct application on complex curved surfaces and structures undergoing large deformation [71]. According to material form and composition, they can be further divided into piezoelectric single crystals, piezoelectric ceramics and inorganic piezoelectric thin films.

3.1.1. Piezoelectric Single-Crystal Substrates

Piezoelectric single crystals are representative early IDT substrates. White and Voltmer reported direct excitation of surface elastic waves using periodic surface electrodes, laying the experimental foundation for IDT acoustic devices [65]. Subsequently, quartz, $LiNbO_3$ and $LiTaO_3$ single crystals were widely used in SAW filters, delay lines and frequency control devices [66,70]. Quartz is known for frequency stability, whereas $LiNbO_3$ and $LiTaO_3$ possess a stronger piezoelectric response and electromechanical coupling and are more suitable for broadband and high-frequency acoustoelectric conversion [71]. In recent years, thin-film $LiNbO_3$ has further promoted IDTs toward high frequency, miniaturization and on-chip integration. GHz-level A_1-mode Lamb-wave devices based on $LiNbO_3$ thin films show advantages in high frequency, low loss and broadband integration [96,98,116,117].

Single-crystal IDTs offer excellent frequency stability, low acoustic loss and strong high-frequency performance. Their limitations are high stiffness and brittleness, which make direct adaptation to curved and flexible structures difficult. For flexible SHM, single-crystal materials usually need to be combined with flexible substrates by thinning, transfer printing or heterogeneous integration. A high-resolution schematic of a representative $LiNbO_3$ thin-film IDT configuration is provided in Figure 4.

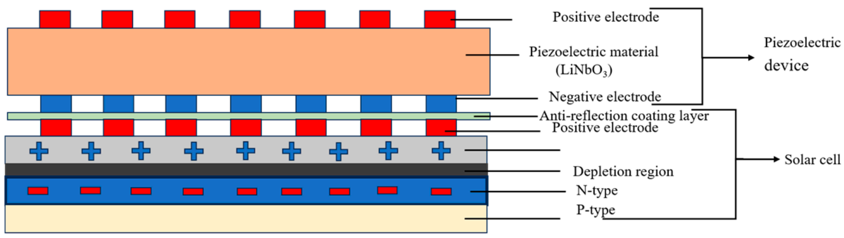

Figure 4. High-resolution schematic of a $LiNbO_3$ thin-film IDT [116].

3.1.2. Piezoelectric Ceramic Substrates

Piezoelectric ceramics have a strong piezoelectric response, high electromechanical coupling efficiency and mature preparation processes. They are commonly used for active excitation and guided-wave detection in IDTs. Compared with single crystals, ceramics can produce a larger mechanical response under relatively low driving voltages and are suitable for Lamb-wave excitation, ultrasonic transduction and active SHM. Typical piezoelectric ceramics include lead zirconate titanate (PZT), barium titanate ($BaTiO_3$), potassium sodium niobate ($(K,Na)NbO_3$, KNN), and bismuth sodium titanate ($Bi_{0.5}Na_{0.5}TiO_3$, BNT).

PZT is one of the most mature ceramic substrates for IDTs. Giurgiutiu investigated tuned Lamb-wave excitation and detection using PZT wafers and showed that the matching among transducer size, excitation frequency and target modal wavelength significantly affects the guided-wave response [80]. Jin et al. designed a PZT-IDT for crack detection in plates and demonstrated that matching the electrode period with the Lamb-wave wavelength can enhance modal selectivity and propagation directivity [81]. Stepinski et al. and

Mańka et al. further developed tunable IDTs by changing electrode connections, enabling switchable excitation of different wavelengths and modes and improving the adaptability of PZT-IDTs in guided-wave inspection [118,119].

Thin-film PZT provides an important route for flexible integration and miniaturized devices. PZT films can be prepared by sol–gel processing, sputtering and micromachining, and have been used in PMUTs, MEMS sensors and flexible ultrasonic transducers [120–123]. Dangi et al. integrated PZT thin films on PI substrates to fabricate flexible PZT ultrasonic transducers, demonstrating that high-response ceramic films can be integrated with flexible substrates to alleviate the rigidity of bulk ceramics [99]. Recent reviews also indicate that PZT thin films remain competitive in MEMS, ultrasonic detection and acceleration sensing, although mechanical stability, process compatibility and environmental considerations still need improvement [100]. A representative flexible PZT thin-film transducer is shown in Figure 5.

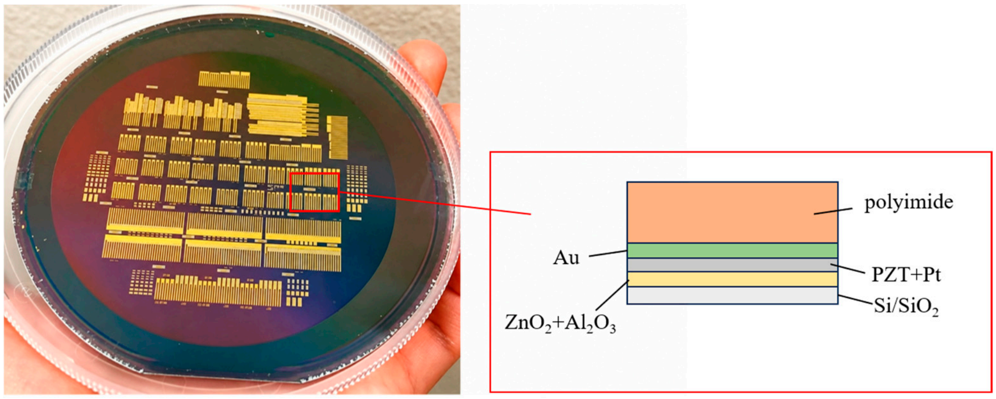

Figure 5. Flexible PZT thin-film ultrasonic transducer: [99].

Lead-free piezoelectric ceramics have also attracted increasing attention. $BaTiO_3$ is lead-free, has a high dielectric constant and can be fabricated using mature processes, but its piezoelectric properties and Curie temperature are generally lower than those of PZT, making it more suitable as a filler in flexible composite sensors [105]. KNN-based ceramics have relatively high Curie temperatures and promising lead-free potential; high piezoelectric performance can be obtained through composition design and phase-boundary regulation [106,109]. BNT-based ceramics show large field-induced strain and are suitable for actuators and large-strain sensing, but their high coercive field and hysteresis limit their use in low-power IDTs [110,111].

Overall, PZT remains suitable for strong guided-wave excitation and active SHM, while $BaTiO_3$, KNN and BNT provide material bases for lead-free and composite designs. The main limitations of ceramic substrates are high stiffness, brittleness and limited conformability to curved surfaces. Thus, in flexible IDTs, ceramics are more suitable as piezoelectric thin films, local reinforcement layers or ceramic/polymer composite phases.

3.1.3. Inorganic Piezoelectric Thin-Film Substrates

AlN, AlScN and ZnO are commonly used inorganic piezoelectric thin-film materials for IDTs. Compared with bulk ceramics, thin films are more compatible with micro/nanofabrication, array fabrication and on-chip integration, and can be combined more easily with silicon, sapphire, glass, metal foils or polymer substrates. AlN/AlScN is particularly suitable for high-frequency, low-loss and on-chip acoustic devices, whereas ZnO is more suited to low-cost flexible SAW devices and multifunctional surface sensing.

AlN has high acoustic velocity, low dielectric loss, good thermal stability and relatively strong CMOS compatibility. It is widely used in high-frequency Lamb-wave resonators, SAW devices and high-temperature sensors [124–126]. Lam et al. studied transducer design for AlN Lamb-wave resonators and pointed out that electrode material, thickness, finger width and film parameters affect electromechanical coupling and device loss [127]. Further studies by Zou et al. on multimode resonance, boundary reflection and low-loss design demonstrate that the performance of AlN-based IDTs depends not only on the piezoelectric film but also on electrode loading, film stack and acoustic boundary conditions [128–131]. Figure 6 provides a representative example of an AlN IDT-based microcantilever device.

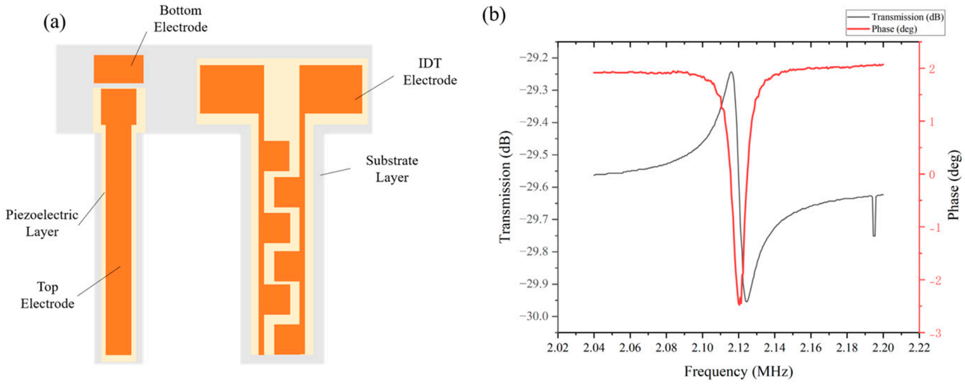

Figure 6. AlN microcantilever humidity sensor excited by IDTs: (**a**) device schematic; (**b**) transmission and phase response near resonance [132].

AlScN represents an important performance-oriented development of conventional AlN piezoelectric thin films. Sc incorporation enhances the electromechanical coupling of AlN and therefore improves the electrical-to-acoustic energy conversion capability of high-frequency acoustic devices [133]. For example, Esteves et al. reported $Al_{0.68}Sc_{0.32}N$ Lamb-wave resonators with an electromechanical coupling coefficient of approximately 10.28% [134]. Compared with conventional AlN, this enhanced coupling makes AlScN particularly attractive for IDTs requiring stronger acoustic excitation, reduced device dimensions, and high-frequency operation.

However, the improvement in electromechanical coupling is accompanied by a trade-off between piezoelectric performance and film stability. Increasing the Sc content may increase film stress, make crystallographic texture more difficult to control, and introduce phase-stability problems. These effects are particularly important for flexible and large-area IDTs, because a film with high electromechanical coupling does not necessarily provide the best device-level performance if excessive residual stress, poor texture uniformity, or structural instability leads to interfacial degradation. Therefore, the optimization of AlScN films should not focus solely on maximizing the Sc concentration or electromechanical coupling coefficient, but should balance coupling performance, film stress, orientation stability, and fabrication uniformity.

The performance of AlScN-based IDTs should also be considered at the film stack and interface levels rather than at the piezoelectric film level alone. Studies on AlN acoustic devices have already shown that electrode loading, film thickness, multilayer configuration, and acoustic boundary conditions can substantially influence electromechanical coupling and acoustic loss [127–131]. These effects may become more pronounced when AlScN films are integrated with flexible substrates, because mechanical mismatch between the piezoelectric layer, electrode, buffer layer, and supporting substrate can interact with the intrinsic film stress. Consequently, the development of flexible AlScN IDTs requires coordinated optimization of the piezoelectric film, electrode/film interface, supporting layer, and acoustic boundary. This material–interface–device co-design represents an important transition from simply increasing intrinsic piezoelectric performance toward achieving stable device-level performance under bending and long-term service.

3.2. Piezoelectric Polymers and Flexible Substrates

Piezoelectric polymers provide a different design route for flexible IDTs. PVDF and its copolymer PVDF-TrFE are lightweight, flexible, corrosion resistant and suitable for large-area processing. Since Kawai discovered the piezoelectricity of PVDF in 1969, PVDF has become a representative material for flexible piezoelectric sensors [135]. Its piezoelectric voltage constant is relatively high, making it suitable for dynamic strain, impact, vibration and acoustic emission detection. In addition, the electroactive phases of PVDF and its copolymers can be regulated by stretching, poling, electrospinning and thin-film processing to improve sensing performance [136–138].

PVDF has good flexibility and attachment capability for structural monitoring. Guzman et al. studied the survivability of integrated PVDF film sensors under accelerated aging conditions in aeronautical and aerospace composite structures and found that the sensors could still provide valid signals after aging [139]. Singh et al. fabricated a lightweight self-powered vibration sensor based on PVDF nanofibers and used it for string vibration measurement, demonstrating the potential of PVDF for miniaturized, low-mass and dynamic-response sensing [140]. BTO/PVDF-HFP composite nanofibers can further improve acoustoelectric output, providing a new material route for broadband acoustoelectric transducers [141].

In IDTs, PVDF or PVDF-TrFE can serve as a piezoelectric layer combined with interdigital electrodes to form flexible transducers. Their advantages include bendability, conformal attachment and suitability for complex surfaces and large-area fabrication. Their limitations are that piezoelectric strain constants and electromechanical coupling are lower than those of PZT, $LiNbO_3$ and AlN, and active guided-wave excitation capability is limited. The viscoelasticity of polymers also introduces significant acoustic loss. For high-temperature or long-term service, PVDF usually requires encapsulation, composite reinforcement or combination with inorganic piezoelectric fillers. A representative PVDF-HFP acoustoelectric transducer is shown in Figure 7.

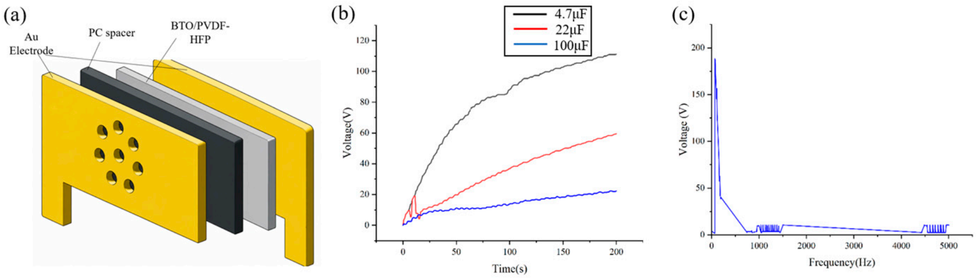

Figure 7. PVDF-HFP acoustoelectric transducer: (**a**) equivalent circuit; (**b**) capacitor voltage as a function of charging time; (**c**) voltage output over the frequency range [141].

PI, PET and PDMS are often used as flexible substrates, encapsulation layers or buffer layers for IDTs. PI has good temperature resistance, dimensional stability and microfabrication compatibility, and is suitable for supporting PZT, AlN and ZnO films. PET is low-cost and suitable for low-cost flexible sensing. PDMS has good stretchability and biocompatibility and is widely used in wearable and soft structures. A flexible substrate does not simply provide mechanical support; its thickness, modulus, acoustic impedance and damping characteristics change the acoustic field distribution and influence bandwidth, frequency response and signal amplitude.

3.3. Piezoelectric Composites and Heterogeneous Integrated Substrates

A single material is often unable to simultaneously satisfy the requirements of high piezoelectric response, low acoustic loss, flexible conformability and environmental stability. Piezoelectric composites and heterogeneous integrated structures have therefore become important directions for flexible IDTs. The former combine inorganic piezoelectric phases with polymer matrices to improve flexibility and actuation capability, while the latter use thin-film deposition, transfer printing, bonding and micro/nanofabrication to realize multilayer functional integration.

3.3.1. Piezoelectric Fiber Composites

Macro-fiber composites (MFCs) and active-fiber composites (AFCs) are typical piezoelectric fiber composites. They generally consist of oriented piezoceramic fibers, a polymer matrix and interdigital electrodes. The interdigital electrodes generate an in-plane electric field along the fiber direction, efficiently utilizing the d_{33} mode to produce strong in-plane actuation. The piezoelectric fiber composite with interdigital electrodes proposed by Bent and Hagood laid the foundation for later MFC/AFC transducers [142]. Wilkie et al. further developed anisotropic piezocomposite actuators based on single-crystal fibers, improving the actuation performance of composite piezoelectric structures [143]. Birchmeier et al., Brunner et al. and Collet et al. investigated piezoelectric fiber composites for Lamb-wave generation, structural monitoring and surface-mounted guided-wave transduction, proving that MFC/AFC can be used for medium- and low-frequency guided-wave excitation and structural state monitoring [144–146]. Representative material properties are compared in Table 1.

Table 1. Comparison of representative material properties of MFC, AFC, PVDF, and PZT.

Relative Permittivity, ε_r	Young's Modulus Along Main (GPa)	d_{33} (pC/N)	Typical Structure	Material
$\approx 10^3$	≈30.3	400–460	Rectangular PZT fibers + epoxy matrix + interdigitated electrodes	MFC
≈755 (ε_{33})	≈21	≈374	Circular PZT fibers + epoxy matrix + interdigitated electrodes	AFC
12–13	2–4	≈ -33	Polarized piezoelectric polymer film	PVDF
1800–3800	49–69	350–650	Bulk piezoelectric ceramic	PZT

MFC/AFC transducers provide stronger actuation than PVDF and better compliance than bulk PZT. They are suitable for composite structures, curved shells and medium- to low-frequency guided-wave monitoring. Lanza di Scalea et al. used MFC transducers to monitor wing skin-to-spar joints of unmanned aerial vehicles and demonstrated the capability of MFCs for Lamb-wave excitation and debonding detection [90]. Mańka et al. further studied tunable MFC-based IDTs and showed that changing electrode connections can adapt the device to different target wavelengths, thereby improving Lamb-wave excitation flexibility [91,147]. Nevertheless, these materials involve complex fabrication and multiple interfaces among fibers, polymer matrices, electrodes and encapsulation layers. Hygrothermal aging, fatigue and thermal cycling may cause interface degradation.

3.3.2. Lead-Free Piezoelectric Composite Films

Lead-free piezoelectric materials provide an important route toward environmentally compatible flexible IDTs, but their role in flexible devices differs from that of conventional bulk ceramic substrates. $BaTiO_3$, KNN, and BNT exhibit different advantages as lead-free piezoelectric phases. $BaTiO_3$ has mature processing and a relatively high dielectric constant but generally lower piezoelectric performance and Curie temperature than PZT [105]. KNN-based ceramics offer relatively high Curie temperatures and can achieve improved piezoelectric properties through composition and phase-boundary regulation [106,109], whereas BNT-based ceramics exhibit large field-induced strain but are constrained by their high coercive field and hysteresis in low-power IDT applications [110,111]. Because these ceramics remain relatively stiff and brittle in bulk form, their integration into polymer matrices is particularly relevant for flexible and conformal IDTs.

The key function of a lead-free composite film is therefore to balance the electromechanical activity of the inorganic phase with the mechanical compliance of the polymer matrix. $BaTiO_3$/PVDF, KNN/PI and related ceramic/polymer systems combine the enhanced piezoelectric or dielectric response of inorganic phases with the flexibility and processability of polymers. BTO/PVDF-HFP composite nanofibers, for example, demonstrate that incorporation of a lead-free piezoelectric phase can improve acoustoelectric output compared with the polymer matrix alone [141]. However, the relationship between ceramic content and device performance is not monotonic. Increasing the inorganic fraction can enhance electromechanical response, but excessive filler loading may increase stiffness, generate additional interface defects and acoustic scattering, and reduce the mechanical durability required for flexible operation. Consequently, the optimization of lead-free composite IDTs should simultaneously consider piezoelectric response, filler content, polarization uniformity, dielectric loss, acoustic impedance matching, and ceramic/polymer interface quality rather than treating the piezoelectric coefficient as the sole material selection criterion. Figure 8 shows a representative flexible PI/BLF-PT device illustrating this integration strategy.

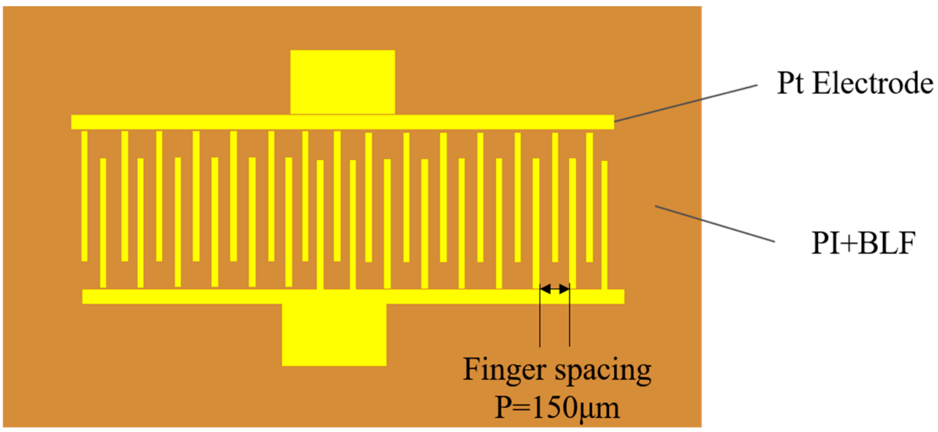

Figure 8. Flexible PI/BLF-PT energy harvester: [148].

3.3.3. Heterogeneous Integrated Substrates

Thin-film heterogeneous integration provides another route. PZT/PI, ZnO/PI, AlN/Si, AlN/sapphire, AlN/metal foil and $LiNbO_3$ thin film/Si structures all belong to this category. This strategy preserves the high-frequency or high-driving characteristics of inorganic piezoelectric films while using substrates, buffer layers and encapsulation to improve mechanical adaptability. Its limitations mainly originate from multilayer mismatch, including differences in thermal expansion coefficient and elastic modulus, residual stress, warpage, interfacial cracks and frequency drift.

3.4. Performance Comparison and Application-Oriented Selection of IDT Substrate Materials

3.4.1. Material-Level Performance Comparison

Different IDT substrate materials exhibit substantial differences not only in intrinsic piezoelectric properties but also in device-level acoustic performance, thermal capability, mechanical compliance and interfacial reliability. Therefore, material selection for IDTs should not be based on a single parameter such as the piezoelectric coefficient or flexibility. Instead, electromechanical coupling, acoustic loss, operating temperature, mechanical durability and integration compatibility should be considered simultaneously.

Piezoelectric single crystals and AlN/AlScN thin films generally provide favorable high-frequency characteristics and relatively low acoustic loss, making them attractive for SAW, Lamb-wave and on-chip acoustic devices. In particular, representative $Al_{0.68}Sc_{0.32}N$ Lamb-wave resonators have demonstrated an electromechanical coupling coefficient of approximately 10.28%, while AlScN-on-SiC resonators have demonstrated operation at temperatures as high as 800 °C. In contrast, PZT and MFC/AFC systems provide stronger actuation capability and are more suitable for active guided-wave excitation and structural health monitoring. Polymer-based and polymer-supported structures, including PVDF, PVDF-TrFE, PZT/PI and ZnO/PI, provide improved conformability but generally involve a trade-off among piezoelectric output, acoustic attenuation and long-term mechanical stability.

Table 2 therefore compares representative substrate systems using engineering-relevant indicators rather than only qualitative advantages and disadvantages. Where a parameter is strongly dependent on device geometry, acoustic mode or testing conditions, it is identified as device-dependent rather than treated as an intrinsic material constant. This distinction is important because device-level performance cannot always be directly inferred from bulk material properties.

Table 2. Engineering-relevant comparison of representative IDT substrate material systems.

Preferred Application	Flexibility/ Durability	Thermal Capability	Acoustic Velocity (m/s)	Relative Permittivity, εr	Electromechanical Performance	Material System
High-frequency SAW/ Lamb-wave; on-chip	Rigid; brittle	~200–500 °C	~3500–7300	~28–50	k_eff^2 ~5–30% (cut/mode dependent)	$LiNbO_3$/$LiTaO_3$ single crystals
Guided-wave SHM; ultrasonic transduction	Bulk: poor; thin-film/PI: moderate–high	~150–300 °C	~3000–4600	~1800–3800	d_{33} ~350–650 pC/N	PZT ceramic/ thin film
Curved/ composite structures; guided-wave SHM	Good conformability; packaging-dependent durability	<150–200 °C	~2500–4000 (effective)	~755–1000	Effective d_{33} ~370–460 pC/N	MFC/AFC
High-frequency resonators; SAW; high-T sensing	Substrate-dependent thin-film flexibility	>500 °C (suitable stacks)	~5500–11,000	~8.5–10	k_eff^2 ~1–3%	AlN thin film
High-coupling on-chip; high-T acoustics	Flexible integration possible; interface stability critical	Up to 800 °C on SiC	~4500–8500	~10–20	k_eff^2 ~5–15%;	AlScN thin film

Table 2. *Cont.*

Preferred Application	Flexibility/ Durability	Thermal Capability	Acoustic Velocity (m/s)	Relative Permittivity, εr	Electromechanical Performance	Material System
Low-cost flexible SAW; multifunctional sensing	Good conformability; device-dependent durability	<200–300 °C	~2700–6000	~8–10	k_eff^2 ~1–5%	ZnO flexible thin film
Curved sensing; wearable/ flexible devices	Excellent flexibility; ~10^3–10^5 bending cycles	<80–120 °C	~1500–2500	~10–13	d_{33} ~−20 to −35 pC/N	PVDF/ PVDF-TrFE

3.4.2. Device-Level Comparison Between Rigid and Flexible IDTs

The advantages of flexible IDTs should be evaluated at the device structure level rather than only through intrinsic material properties. Rigid piezoelectric IDTs, particularly those based on bulk PZT or single-crystal substrates, generally provide strong electromechanical conversion, stable electrode geometry and mature fabrication. On flat structures under well-controlled bonding conditions, such devices may provide higher or more stable guided-wave excitation than polymer-based flexible IDTs.

Flexible IDTs, however, provide advantages that become increasingly important when the monitored structure departs from a flat and mechanically stable configuration. Their lower bending stiffness allows the active area to conform to curved shells, pipelines and composite skins, reducing local gaps and facilitating distributed array deployment. Therefore, the principal advantage of flexible IDTs is not necessarily a higher intrinsic electromechanical conversion efficiency, but improved conformability, reduced structural perturbation, lower added stiffness and more adaptable sensor array integration.

A meaningful comparison between rigid and flexible IDTs should therefore include at least three categories of device-level performance. The first is guided-wave excitation and reception performance, including signal amplitude, signal-to-noise ratio, target mode selectivity and propagation distance under identical excitation conditions. The second is damage detection performance, including damage localization error, imaging contrast, identification accuracy and repeatability. The third is service durability, including bending radius, cyclic bending life, frequency drift, signal retention and interfacial integrity.

Importantly, these indicators should be evaluated under comparable operating conditions. Differences in driving voltage, center frequency, transducer area, host structure, adhesive layer and propagation distance can otherwise dominate the measured response and obscure the actual effect of substrate flexibility. Therefore, future comparative studies should prioritize controlled rigid–flexible benchmarking rather than comparing isolated performance values reported under different experimental configurations.

From an engineering perspective, rigid and flexible IDTs should be regarded as complementary rather than mutually exclusive technologies. Rigid IDTs remain advantageous when high actuation efficiency and dimensional stability dominate, whereas flexible IDTs become increasingly attractive for curved structures, lightweight monitoring, dense arrays and mechanically adaptive interfaces.

3.4.3. Application-Oriented Material Selection Framework

Based on the preceding comparison, substrate selection should be driven by the dominant engineering constraint rather than by a universal material ranking. High-frequency and on-chip applications prioritize electromechanical coupling, acoustic loss and fabrication compatibility, whereas guided-wave SHM emphasizes excitation capability and modal control. Curved-structure monitoring additionally requires mechanical conformability and stable interfacial coupling, while high-temperature applications are governed by thermal stability and multilayer reliability. Stretchable systems further require the interdigital geometry and electrical continuity to remain stable under large deformation. Figure 9 summarizes these application-oriented material selection pathways.

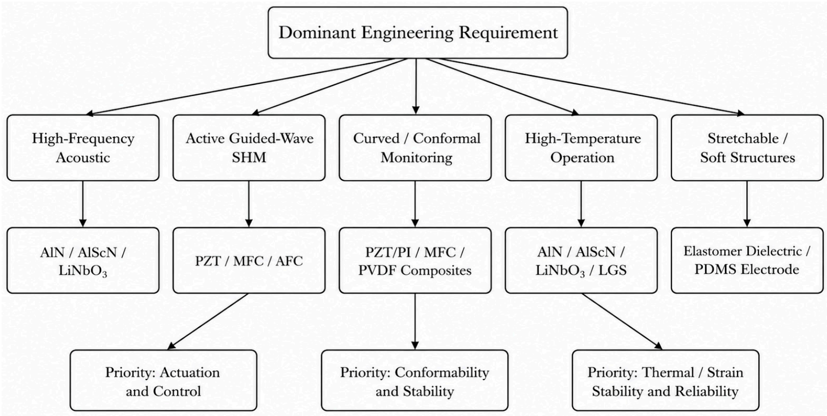

Figure 9. Application-oriented material selection framework for representative IDT substrate systems.

4. Development Trends and Key Issues of IDT Substrate Materials

The rapid development of flexible electronics, thin-film piezoelectric processes, micro/nanofabrication and SHM has driven IDT substrate materials from conventional rigid piezoelectric materials toward thin-film, composite, flexible and highly stable systems.

4.1. High-Temperature Service and Thermal Stability

High temperature changes the dielectric constant, elastic constants and piezoelectric coefficients of materials, further affecting guided-wave velocity, center frequency and signal amplitude. For aerospace engines, gas turbines, high-temperature pipelines, nuclear equipment and bolt preload monitoring, IDTs must maintain detectable acoustoelectric responses at high temperatures and preserve frequency repeatability and signal stability after thermal cycling or long-term exposure. Temperature variation has been shown to change Lamb-wave velocity, phase and amplitude, thereby interfering with damage identification [87,149]. Therefore, high-temperature IDTs should be designed by considering the thermal stability of the piezoelectric layer, electrodes, buffer layer and encapsulation materials simultaneously.

In addition to the intrinsic thermal stability of individual materials, thermal expansion mismatch across multilayer interfaces is a fundamental reliability issue for high-temperature flexible IDTs. For a piezoelectric film/substrate system, the thermal mismatch can be characterized by the difference in thermal expansion coefficients,

$$\Delta\alpha = \alpha_{piezo} - \alpha_{sub} \tag{9}$$

and the corresponding mismatch strain increases approximately with temperature variation as

$$\varepsilon_{th} \propto \Delta\alpha\Delta T \tag{10}$$

Therefore, repeated heating and cooling can generate cyclic tensile and compressive stresses in the piezoelectric layer, electrodes, buffer layers and bonding interfaces. In multilayer flexible devices, these stresses may accumulate near interfaces and promote local cracking, warpage or delamination. Such damage can subsequently alter the mechanical boundary conditions of the IDT and cause changes in acoustic velocity, electromechanical coupling, signal amplitude and center frequency.

Electrode degradation is another key issue for high-temperature IDTs. Conventional metal electrodes are prone to oxidation, diffusion, agglomeration and increased resistance at high temperatures, leading to degradation of the interdigital structure and output attenuation. Pt, Ir, Ru, Pt-Al_2O_3 composite electrodes and high-temperature conductive ceramic electrodes are important options for high-temperature SAW and IDT devices [150]. Pei et al. proposed Pt-Al_2O_3 composite nano-thick interdigital electrodes that showed good thermal stability in SAW sensors, providing a reference for high-temperature electrode design [151]. In addition, AlScN-on-SiC resonators operating up to 800 °C indicate that heterogeneous integration of piezoelectric films with thermally conductive and stable substrates can further extend IDT applications in extreme environments [152].

Electrode degradation and interfacial degradation should therefore be treated as coupled rather than independent high-temperature failure mechanisms. Oxidation, interdiffusion and agglomeration of metal electrodes increase electrical resistance, whereas thermal mismatch can simultaneously weaken adhesion between the electrode, piezoelectric film and supporting substrate. Consequently, high-temperature reliability should be evaluated using not only the maximum operating temperature but also thermal-cycle number, high-temperature holding time, frequency shift, signal amplitude retention, electrode-resistance variation and post-test interfacial morphology.

AlN, AlScN, $LiNbO_3$, $LiTaO_3$, langasite (LGS) and $GaPO_4$ remain important candidate materials for high-temperature acoustic devices. AlN has high acoustic velocity, low dielectric loss and good thermal stability, and has been widely used in high-temperature Lamb-wave resonators, SAW sensors and thin-film ultrasonic transducers [125,153]. Zou et al. investigated the temperature stability of SiO_2/AlN/SiO_2 multilayer Lamb-wave resonators and showed that temperature-induced frequency drift can be regulated through layer-stack design [154]. Moutaouekkil et al. introduced ribbon-structured SiO_2 films into AlN-based Lamb-wave devices and combined them with diamond films to improve velocity and coupling, further indicating that high-temperature stability can be achieved through structural configuration rather than relying only on a single piezoelectric material [92].

In general, high-temperature IDTs need to address three issues: stability of the piezoelectric layer under high temperature, oxidation and diffusion of metal electrodes and interface layers, and coupling between temperature-induced frequency drift and damage signals. Future studies should strengthen systematic evaluation of thermal cycling, long-term heat exposure, frequency drift rate, signal retention rate and interfacial damage morphology.

4.2. High Sensitivity, Low Loss and Modal Control

The detection capability of an IDT depends on whether it can efficiently excite the target wave mode and complete acoustoelectric conversion with low loss. In guided-wave SHM, sensors must detect local defects such as cracks, delamination, debonding and corrosion over relatively large areas. In high-frequency acoustic devices, quality factor, electromechanical coupling coefficient, insertion loss and frequency selectivity are more important. Although the evaluation indicators differ, both applications require good matching among the piezoelectric material, target wave mode, electrode structure and acoustic boundary.

A high piezoelectric response remains the basis for improving IDT conversion efficiency. PZT, PMN-PT, PIN-PMN-PT and MFC/AFC materials provide strong electromechanical conversion and are suitable for active guided-wave excitation and high-sensitivity detection [80,81,118]. In guided-wave inspection, IDTs realize modal selection by matching the finger period with the target wavelength. The PZT-IDT designed by Jin et al. showed that wavelength-period matching enhances the excitation efficiency and propagation directivity of the target mode [81]. Tunable PZT-IDTs and MFC-IDTs proposed by Mańka et al. further confirmed that changing electrode connections or interdigital structures can realize switchable excitation at different wavelengths and frequencies [118,119].

Low-loss design also depends on device structure. For AlN and AlScN Lamb-wave resonators, electrode thickness, metallization ratio, finger width, film thickness and boundary reflection conditions affect electromechanical coupling and acoustic loss [124,127,133]. Zou et al. achieved low-loss AlN Lamb-wave resonators by controlling boundary reflection and acoustic loss, confirming the importance of boundary design for improving the quality factor [129,130]. AlScN further improves the coupling of AlN-based films. The $Al_{0.68}Sc_{0.32}N$ Lamb-wave resonators reported by Esteves et al. achieved a coupling coefficient close to 10.28%, showing that Sc doping can significantly enhance the conversion efficiency of AlN-based films [134]. However, a high Sc content may introduce stress, orientation-control difficulty and phase-stability issues, particularly in large-area fabrication and flexible integration.

Modal control is an important feature that distinguishes IDTs from ordinary piezoelectric patches. By tuning finger period, aperture, number of electrode pairs, phase distribution and array layout, IDTs can enhance target Lamb-wave modes and suppress spurious modes. Frequency-tunable and direction-controllable guided-wave transducers have recently attracted attention. Mohammadgholiha et al. proposed a unidirectional frequency-steerable acoustic transducer for guided-wave damage imaging, showing the potential of electrode and array design for wave-field control [97]. Future improvements in IDT performance will therefore rely not only on high-performance substrates but also on electrode topology, wave-field regulation and signal processing.

4.3. Flexible Attachment and Curved-Structure Adaptation

Flexible IDTs are driven by the needs of curved-structure monitoring, wearable sensing and lightweight equipment monitoring. For aerospace composite skins, pipelines, wind turbine blades and complex curved shells, rigid piezoelectric patches may be difficult to attach stably and may change the local dynamics of the host structure. Flexible substrates reduce device stiffness, improve conformal attachment and facilitate array deployment. PVDF, PVDF-TrFE, ZnO/PI, PZT/PI, AlN/metal foil and MFC/AFC structures all show different levels of flexibility. For curved structures, adhesive thickness, interfacial acoustic impedance and installation consistency significantly affect guided-wave energy transfer.

PZT/PI and ZnO/PI are representative thin-film flexible structures. PZT/PI is more suitable for miniature ultrasonic emission and active excitation, while ZnO/PI is more suitable for low-cost flexible SAW devices and multifunctional sensing. Flexible PZT thin-film transducers on PI substrates demonstrate that high-actuation piezoelectric films can be integrated with flexible substrates for miniature ultrasonic emission and reception [99]. However, the mismatch in elastic modulus and thermal expansion coefficient between inorganic films and polymer substrates may lead to interfacial debonding, electrode cracking and signal drift after cyclic bending. Evaluation of flexible IDTs should therefore include bending radius, number of bending cycles, frequency shift after bending, signal amplitude retention and interface morphology, rather than only initial frequency response and sensitivity.

For curved-structure monitoring, the flexible IDT, adhesive layer and host structure form a coupled multilayer acoustic transfer system. The acoustic impedance of each layer can be expressed as

$$Z = \rho c \tag{11}$$

where ρ is density and c is acoustic velocity. A large impedance mismatch between adjacent layers increases reflection and reduces the acoustic energy transmitted from the IDT to the monitored structure. Therefore, conformability alone does not guarantee efficient guided-wave excitation; the acoustic compatibility of the interface must also be considered.

The adhesive layer plays a dual mechanical and acoustic role. A sufficiently compliant adhesive can improve conformal contact on curved surfaces, whereas excessive adhesive thickness may increase viscoelastic damping and alter the effective mechanical boundary condition of the transducer. The transmitted guided-wave amplitude can therefore be regarded as a coupled function of adhesive thickness h_a, adhesive modulus E_a, interfacial acoustic impedance Z_a, excitation frequency f, and structural curvature R:

$$A_{trans} = F(h_a, E_a, Z_a, f, R) \tag{12}$$

This expression is introduced here as an engineering framework rather than a universal closed-form law, because the exact relationship depends on the guided-wave mode, frequency–thickness product, adhesive viscoelasticity and structural geometry. Nevertheless, it highlights that curved-surface IDT optimization should simultaneously consider mechanical conformity and acoustic energy transfer.

Accordingly, future curved-surface IDT studies should report not only bending radius and signal amplitude but also adhesive thickness, attachment pressure, interface condition and signal repeatability. Such information is required to distinguish improvements caused by the substrate material itself from those caused by installation and interfacial coupling.

Flexible SAW devices provide important references for flexible IDTs [155–158]. Jin et al. built flexible SAW resonators on plastic films, showing that ZnO films can realize acoustoelectric conversion on flexible substrates [155]. He et al. fabricated dual-mode flexible SAW devices based on ZnO/PI and used them for ultraviolet sensing [156]. Wu et al. constructed flexible transparent humidity sensors using ultrathin glass, ZnO nanowires and graphene quantum dots, demonstrating the potential of flexible acoustic devices for environmental detection [158]. Recent reviews of flexible SAW and wearable acoustic devices indicate that flexible acoustic devices have been developed for temperature, humidity, ultraviolet, strain and physiological signal detection, but the acoustic propagation theory under bending strain, long-term device stability and batch-to-batch consistency still require further study [94,159,160].

Curved-structure SHM imposes higher requirements on flexible IDTs than ordinary flexible sensing. Wearable sensing often focuses on local strain or surface disturbance, whereas large-scale guided-wave monitoring requires stronger excitation, longer propagation distance and repeatable interface coupling under curvature. Therefore, design experience from flexible SAW devices cannot be transferred directly to guided-wave SHM. Future research should establish clearer relationships among material flexibility, acoustic output, structural curvature and long-term interface coupling stability.

4.4. Stretchable Devices and Soft-Structure Applications

Flexible devices mainly solve bending adaptation, whereas stretchable devices further require electrical continuity and stable acoustic response under stretching, compression, torsion and large deformation. The development of soft robots, electronic skins, human–machine interaction and wearable systems has made stretchable interdigital structures a new research direction. Dielectric elastomers, PDMS, Ecoflex, liquid metals, carbon nanomaterials and conductive polymers are commonly used in this field. The deformation principle of a dielectric elastomer transducer is illustrated in Figure 10.

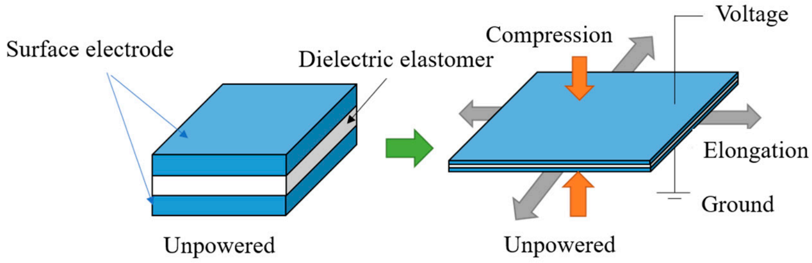

Figure 10. Deformation principle of a dielectric elastomer (DE) transducer.

Dielectric elastomers have large deformation, low density and fast response, and are suitable for soft actuation and large-deformation sensing. Pelrine et al. demonstrated the potential of dielectric elastomers for electrostrictive actuation and later reported high-speed electrically actuated elastomers with strain greater than 100% [161,162]. Subsequent studies indicated that dielectric elastomer transducer performance depends on dielectric constant, elastic modulus, breakdown strength, electrode compliance and charge leakage [163–165]. Bar-Cohen and Anderson reviewed electroactive polymer actuators and pointed out that such materials are advantageous for compliant actuation, although driving voltage, material stability and long-term performance still limit their applications [95].

For clarity, EAP, EAC and SMA denote electroactive polymer, electroactive ceramic and shape memory alloy, respectively. Table 3 reports actuation strain quantitatively and describes the different actuator classes using directly comparable mechanical response terms.

Table 3. Comparison of electroactive polymers and selected traditional actuator materials.

Typical Mechanical Response	Response Time (s)	Stress (MPa)	Actuation Strain	Material Type
Large, recoverable elastic deformation	~10^{-6}	0.1–25	Up to >100% (DE-type EAPs)	Electroactive polymer (EAP) [95]
Small-strain, high-stress response; limited flexibility	~10^{-3}	30–40	0.1–0.3%	Electroactive ceramic (EAC) [163]
Recoverable strain through phase transformation	~10^{-3}–60	~200	<8%	Shape memory alloy (SMA) [165]

For stretchable IDTs, the main challenge is not only maintaining electrical continuity but also preserving the periodic geometry that determines acoustic frequency selection. Conventional metal electrodes can crack under large deformation, resulting in increased resistance and eventual failure of the interdigital structure. Conductive polymers, carbon-based electrodes and ionic conductors provide improved mechanical compliance, although their resistance stability, high-frequency response and environmental durability remain important limitations. The transparent ionic conductors reported by Keplinger et al. provide a representative strategy for mechanically compliant electrodes [166], while the 3D-printed interdigitated dielectric elastomer actuators demonstrated by Chortos et al. show that complex stretchable interdigital geometries can be fabricated [167].

More importantly, mechanical deformation directly modifies the frequency-selective geometry of an IDT. According to the frequency-matching relationship introduced in Section 2, the center frequency is determined by the acoustic velocity and interdigital wavelength, f0 = v/λ. When an interdigital structure is stretched, both the finger spacing and the effective acoustic wavelength may change. For a small perturbation, the resulting relative frequency shift can be expressed approximately as

$$\frac{\Delta f}{f0} \approx \frac{\Delta v}{v} - \frac{\Delta \lambda}{\lambda} \tag{13}$$

This relationship shows that the frequency drift of a stretchable IDT originates from two coupled effects: deformation-induced changes in acoustic velocity and changes in the periodic electrode geometry. When the variation in acoustic velocity is relatively small, geometric deformation of the interdigital period becomes the dominant contribution to the center frequency shift. Therefore, a stretchable IDT must maintain not only electrode conductivity but also geometric periodicity during cyclic deformation.

From this perspective, three coupled stability requirements should be considered for stretchable interdigital devices: electrical stability of the compliant electrodes, geometrical stability of the finger period, and acoustomechanical stability of the piezoelectric/substrate interface. Accordingly, future characterization should not be limited to the maximum achievable strain. Frequency shift under strain, electrical resistance variation, signal amplitude retention, cyclic deformation life, and recovery of the interdigital geometry should also be reported. These metrics are particularly important when stretchable interdigital structures are extended from soft actuation and wearable sensing toward guided-wave excitation and structural monitoring.

At present, stretchable IDTs are still at an early stage of development for large engineering SHM. They are more suitable for soft-structure state monitoring, low-frequency vibration detection, flexible interface perception and wearable systems. If used for guided-wave inspection, they must provide sufficient acoustic output, a stable interdigital period and repeatable interface coupling. In the short term, stretchable interdigital structures are more likely to supplement flexible IDTs than to replace mature transduction systems such as PZT, MFC/AFC, AlN or $LiNbO_3$.

4.5. Representative Flexible IDT Designs and System-Level Demonstrations

Representative studies from our research group illustrate how flexible substrate design can be combined with electrode topology and array configuration. A ring-shaped broadband omnidirectional IDT and its array were constructed using a PVDF/PDMS composite flexible substrate. By optimizing interdigital parameters and annular array configurations, multifrequency guided-wave responses, directional characteristics and damage localization capability were demonstrated [168]. The main contribution of this design is the integration of substrate conformability with omnidirectional array-level wave-field control.

On this basis, a plum-blossom-shaped interdigital guided-wave transducer based on an Archimedean spiral was proposed by combining sector-shaped interdigital units with annular arrays, enabling broadband and omnidirectional guided-wave excitation and reception for plate damage imaging [169]. This design further demonstrates that flexible substrate performance can be enhanced through coordinated optimization of electrode geometry and spatial array layout rather than by material selection alone.

At the system level, a $LiNbO_3$/Al-based SAW temperature sensor and a GNU Radio wireless interrogation platform were developed for remote temperature-signal extraction and calibration [170]. Together, these studies show a progression from flexible substrate selection to wave-field regulation and system-level wireless integration. Representative array and system-level implementations are summarized in Figure 11.

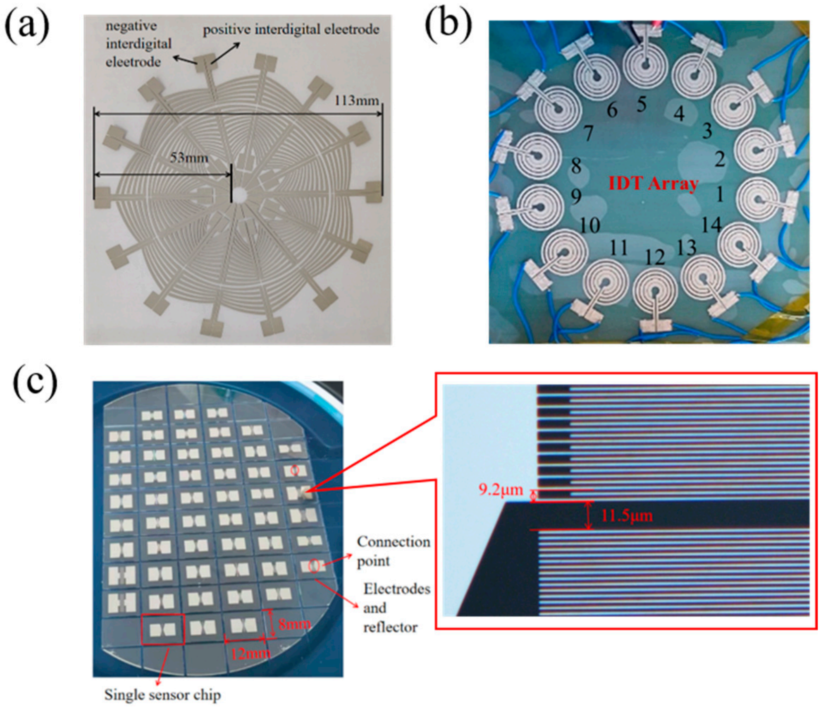

Figure 11. Fundamentals of IDTs and SAW sensor fabrication: (**a**) flexible fan-shaped IDTs and their plum blossom-shaped array; (**b**) annular IDT array fabricated on a PVDF/PDMS substrate; and (**c**) the $LiNbO_3$/Al-based SAW sensor and its microstructure [168–170].

Despite these advances, several limitations remain. Most current demonstrations have been performed under laboratory conditions and on relatively regular plate-like structures. Systematic comparisons with conventional rigid IDTs under identical excitation, bonding and propagation conditions remain limited, and long-term durability under cyclic bending, thermal cycling and hygrothermal aging has not yet been fully established. Further validation on complex curved engineering structures, together with system-level optimization of wiring, packaging, channel synchronization and multichannel or wireless interrogation, is therefore required before these flexible array concepts can be translated into deployable SHM systems.

These case studies reinforce the broader conclusion that flexible IDT development requires coordinated optimization of substrate properties, electrode topology, interface coupling and system integration rather than improvement in any single material parameter in isolation.

5. Conclusions and Outlook

This review summarizes the research progress of substrate materials for flexible interdigital transducers, focusing on piezoelectric single crystals, PZT, AlN/AlScN, ZnO, PVDF, MFC/AFC, composite substrates and heterogeneous integrated structures. Different substrates show clear differences in electromechanical coupling efficiency, acoustic loss, flexible conformability, temperature stability and long-term service performance. Piezoelectric single crystals and AlN/AlScN thin films are suitable for high-frequency, low-loss and on-chip acoustic devices.

Current studies show that IDT substrate materials face three major limitations. First, high piezoelectric performance and flexible conformability are still difficult to achieve simultaneously. Inorganic piezoelectric materials have high conversion efficiency but high stiffness and brittleness, whereas polymers are flexible but limited in actuation capability and temperature resistance. Second, composite and heterogeneous integrated structures can compensate for the limitations of single materials, but residual stress, thermal mismatch, debonding and fatigue failure at multiple interfaces remain important issues. Third, many studies still focus on single-device performance demonstration and lack systematic evaluation under long-term service conditions, including thermal cycling, hygrothermal aging, cyclic bending, interface degradation and signal drift.

Future studies on IDT substrate materials should pay more attention to application-oriented material selection and device design. Five directions are particularly important: (1) high-coupling flexible thin films and lead-free composites that better balance electromechanical output with mechanical compliance; (2) interface engineering for electrodes, piezoelectric layers, buffer/adhesive layers and flexible supports to suppress residual stress, debonding and fatigue; (3) long-term reliability under high temperature, thermal cycling, hygrothermal aging and repeated bending; (4) deformation-tolerant electrode architectures and compensation strategies that preserve interdigital periodicity and frequency stability in stretchable devices; and (5) standardized rigid–flexible benchmarking under identical driving, bonding and structural conditions, using unified metrics such as coupling efficiency, acoustic loss, damage localization accuracy and service life. Overall, flexible IDT substrate materials are developing toward thin-film, composite, flexible, thermally stable and system-integrated forms. Future research needs to shift from comparing single material properties to validating device-level and structure-level performance, establish unified evaluation metrics and consider long-term stability in practical service environments. With the progress of thin-film deposition, micro/nanofabrication, transfer printing and flexible encapsulation, IDT substrate materials are expected to find broader applications in SHM, extreme-environment sensing, intelligent equipment and flexible electronics. From a structural symmetry perspective, future substrate development should not only improve piezoelectric response, flexibility, thermal stability and interfacial reliability, but also help maintain the periodic regularity and stable frequency-selective response of IDTs during practical service.

Author Contributions: Conceptualization, Z.W. and H.Z.; Methodology, Z.W. and C.W.; Software, X.W. and A.G.; Validation, Z.W. and H.Z.; Formal Analysis, Z.W. and N.R.T.; Investigation, Z.W.; Writing—Original Draft Preparation, H.Z.; Writing—Review and Editing, Z.W. and C.W.; Funding Acquisition, Z.W. All authors have read and agreed to the published version of the manuscript.

Funding: This work was supported by the Foreign Experts Program of the Ministry of Science and Technology (No. 110000218020258051) and the National Natural Science Foundation of China (No. 92471203 and No. 11872191).

Data Availability Statement: Representative processed data and the main imaging parameter settings used in this study are available from the corresponding author upon reasonable request.

Conflicts of Interest: The authors declare no conflicts of interest.

References

1. Giordano, P.F.; Quqa, S.; Limongelli, M.P. The value of monitoring a structural health monitoring system. *Struct. Saf.* **2023**, *100*, 102280. [CrossRef]
2. Raghavan, A.; Cesnik, C.E.S. Review of guided-wave structural health monitoring. *Shock Vib. Dig.* **2007**, *39*, 91–114. [CrossRef]
3. Mao, H.; Du, X.; Yan, Y.; Zhang, X.; Ma, G.; Wang, Y.; Liu, Y.; Wang, B.; Yang, X.; Shi, Q. Highly sensitive detection of daminozide using terahertz metamaterial sensors. *Int. J. Agric. Biol. Eng.* **2022**, *15*, 180–188. [CrossRef]
4. Shoaib, M.; Li, H.; Zareef, M.; Khan, I.M.; Iqbal, M.W.; Niazi, S.; Raza, H.; Yan, Y.; Chen, Q. Recent advances in food safety detection: Split aptamer-based biosensors development and potential applications. *J. Agric. Food Chem.* **2025**, *73*, 4397–4424. [CrossRef]
5. Zhang, Z.; Zhang, Y.; Jayan, H.; Gao, S.; Zhou, R.; Yosri, N.; Zou, X.; Guo, Z. Recent and emerging trends of metal-organic frameworks (MOFs)-based sensors for detecting food contaminants: A critical and comprehensive review. *Food Chem.* **2024**, *448*, 139051. [CrossRef]

6. Su, Z.; Ye, L.; Lu, Y. Guided Lamb waves for identification of damage in composite structures: A review. *J. Sound Vib.* **2006**, *295*, 753–780. [CrossRef]
7. Giurgiutiu, V. *Structural Health Monitoring with Piezoelectric Wafer Active Sensors*, 2nd ed.; Academic Press: Oxford, UK, 2014.
8. Cawley, P.; Alleyne, D. The use of Lamb waves for the long range inspection of large structures. *Ultrasonics* **1996**, *34*, 287–290. [CrossRef]
9. Xu, Y.; Kutsanedzie, F.Y.H.; Sun, H.; Wang, M.; Chen, Q.; Guo, Z.; Wu, J. Rapid Pseudomonas species identification from chicken by integrating colorimetric sensors with near-infrared spectroscopy. *Food Anal. Methods* **2018**, *11*, 1199–1208. [CrossRef]
10. Fromme, P.; Wilcox, P.; Cawley, P. Remote monitoring of plate-like structures using guided wave arrays. *AIP Conf. Proc.* **2003**, *657*, 157–164. [CrossRef]
11. Wilcox, P.D. Omni-directional guided wave transducer arrays for the rapid inspection of large areas of plate structures. *IEEE Trans. Ultrason. Ferroelectr. Freq. Control* **2003**, *50*, 699–709. [CrossRef]
12. Liang, Z.; Li, Y.; Zhao, Z. Monitoring method and sensor for grain separation loss on axial flow combine harvester. *Trans. Chin. Soc. Agric. Eng.* **2014**, *30*, 18–26.
13. Huo, X.; Liu, B.; Wu, Z. Recent advances of flexible pressure tactile sensors: Sensing mechanisms, performance breakthroughs, and intelligent applications. *Adv. Mater. Technol.* **2026**, *11*, e01837. [CrossRef]
14. Wang, T.; Xie, L.; Xing, J.; Zhu, X. Design and analysis of a novel SAW sensor for civil structural health monitoring. *Integr. Ferroelectr.* **2017**, *183*, 8–18. [CrossRef]
15. Jing, Z.; Ding, J.; Zhang, T.; Yang, D.; Qiu, F.; Chen, Q.; Xu, J. Flexible, versatility and superhydrophobic biomass carbon aerogels derived from corn bracts for efficient oil/water separation. *Food Bioprod. Process.* **2019**, *115*, 134–142. [CrossRef]
16. Yao, K.; Sun, J.; Cheng, J.; Xu, M.; Chen, C.; Zhou, X. Nondestructive detection of s-ovalbumin content in eggs using portable nir spectrometer and mpa-cars. *J. Food Process Eng.* **2023**, *46*, e14186. [CrossRef]
17. Wu, W.; Zeng, T.; Hao, W.; Jiang, S. Microstructure and Mechanical Properties of Aluminum Matrix Composites Reinforced with In-Situ TiB_2 Particles. *Front. Mater.* **2022**, *9*, 817376. [CrossRef]
18. Damage Analysis of Carbon Fiber-Reinforced Thermoplastic Laminates under Bending Based on Acoustic Emission Digital Image Correlation. *J. Mater. Eng. Perform.* **2024**, *33*, 1411–1423. [CrossRef]
19. Liu, H.; Zhu, H. Evaluation of a laser scanning sensor in detection of complex-shaped targets for variable-rate sprayer development. *Trans. ASABE* **2016**, *59*, 1181–1192. [CrossRef]
20. Liu, Z.; Liu, G.; Qiao, J. Laser ranging sensor for apple harvesting robot. *J. Jiangsu Univ. (Nat. Sci. Ed.)* **2010**, *31*, 373–377.
21. Li, Z.; Ma, L.; Han, C.; Wang, S. Obstacle detection method of lawn mowing robot based on multi-sensor fusion. *J. Jiangsu Univ. (Nat. Sci. Ed.)* **2024**, *45*, 160–166.
22. Li, L.; Xie, S.; Zhu, F.; Ning, J.; Chen, Q.; Zhang, Z. Colorimetric sensor array-based artificial olfactory system for sensing Chinese green tea's quality: A method of fabrication. *Int. J. Food Prop.* **2017**, *20*, 1762–1773. [CrossRef]
23. Meiqing, L.; Jinyang, L.; Xinhua, W.; Wenjing, Z. Early diagnosis and monitoring of nitrogen nutrition stress in tomato leaves using electrical impedance spectroscopy. *Int. J. Agric. Biol. Eng.* **2017**, *10*, 194–205.
24. Liang, Z.; Li, Y.; Xu, L.; Zhao, Z.; Tang, Z. Optimum design of an array structure for the grain loss sensor to upgrade its resolution for harvesting rice in a combine harvester. *Biosyst. Eng.* **2017**, *157*, 24–34. [CrossRef]
25. Liu, B.; Zheng, H.; Lin, Y.; Liu, S.; Zheng, H.; You, C.; Shi, H.; Lan, J.; Li, Z.; Tang, J.; et al. Design of Environmental Monitoring and Control System for Large-scale Pig House with Fermentation Bed. *Agric. Sci. Technol.* **2015**, *16*, 391.
26. Rong, Y.; Hassan, M.M.; Ouyang, Q.; Chen, Q. Lanthanide ion (Ln^{3+})-based upconversion sensor for quantification of food contaminants: A review. *Compr. Rev. Food Sci. Food Saf.* **2021**, *20*, 3531–3578. [CrossRef]
27. Xu, Y.; Hassan, M.M.; Sharma, A.S.; Li, H.; Chen, Q. Recent advancement in nano-optical strategies for detection of pathogenic bacteria and their metabolites in food safety. *Crit. Rev. Food Sci. Nutr.* **2023**, *63*, 486–504. [CrossRef]
28. Xu, M.; Wang, Z.; Niu, X.; Wang, Z.; Zou, W.; Zhai, C.; Li, S. Design and Research of Soil Disinfection Pesticide Application Control System Based on PSO-PID Algorithm. *Agriculture* **2026**, *16*, 481. [CrossRef]
29. Salam, A.; Khan, S.M.; Afridi, M.S.; Khan, A.R.; Zeeshan, M.; Rehman, M.; Wu, H.; Iqbal, A.; Zhang, Z.; Zhao, C. Recent Advances in Nanomaterial-Based Approaches for Plant Disease Management and Early Detection. *J. Agric. Food Chem.* **2026**, *74*, 7322–7349. [CrossRef]
30. Zaman, A.; Alkulify, F.; BaQais, A.; Alsolami, A.; Alfihed, S.; Guneroglu, U.; Li, L.; Alshamrani, N.; Wang, J. Generation of Clean and Renewable Energy through Compatible Piezoelectric Devices Based on NbO_3 Material. *ACS Omega* **2026**, *11*, 23779–23794. [CrossRef] [PubMed]
31. Yu, Z.; Yue, Y.; Liang, Z.; Zhao, X.; Li, F.; Peng, W.; Zhu, Q.; He, Y. Physical sensors based on Lamb wave resonators. *Micromachines* **2024**, *15*, 1243. [CrossRef]
32. Gao, J.; Zhang, J.; Lu, D. Design and atomization experiments of an ultrasonic atomizer with a levitation mechanism. *Appl. Eng. Agric.* **2016**, *32*, 353–360. [CrossRef]

33. Zhang, Y.; Xu, L.; Rui, X.; Qi, L.; Shi, N.; Li, X.; Li, J. Research on continuous ultrasonic source localization of composite structures by frequency domain characteristics indexing. *Measurement* **2022**, *192*, 110930. [CrossRef]
34. Han, F.; Huang, X.; Teye, E. Novel prediction of heavy metal residues in fish using a low-cost optical electronic tongue system based on colorimetric sensors array. *J. Food Process Eng.* **2019**, *42*, e12983. [CrossRef]
35. Wang, J.; Zhang, Y.; Gu, R. Research status and prospects on plant canopy structure measurement using visual sensors based on three-dimensional reconstruction. *Agriculture* **2020**, *10*, 462. [CrossRef]
36. Kutsanedzie, F.Y.; Agyekum, A.A.; Annavaram, V.; Chen, Q. Signal-enhanced SERS-sensors of CAR-PLS and GA-PLS coupled AgNPs for ochratoxin A and aflatoxin B1 detection. *Food Chem.* **2020**, *315*, 126231. [CrossRef]
37. Han, F.; Huang, X.; Aheto, J.H.; Zhang, D.; Feng, F. Detection of beef adulterated with pork using a low-cost electronic nose based on colorimetric sensors. *Foods* **2020**, *9*, 193. [CrossRef]
38. Wang, Z.; Li, B.; Cui, H.; Güemes, A.; Fernández-López, A.; Gorgin, R. Damage imaging method based on circular DE-IDT array for phased array data fusion. *Struct. Health Monit.* **2023**, *23*, 2531–2541. [CrossRef]
39. Pan, C.T.; Chang, C.C.; Yang, Y.S.; Yen, C.K.; Kao, Y.H.; Shiue, Y.L. Development of MMG sensors using PVDF piezoelectric electrospinning for lower limb rehabilitation exoskeleton. *Sens. Actuators A Phys.* **2020**, *301*, 111708. [CrossRef]
40. Sharma, A.S.; Ali, S.; Sabarinathan, D.; Murugavelu, M.; Li, H.; Chen, Q. Recent progress on graphene quantum dots-based fluorescence sensors for food safety and quality assessment applications. *Compr. Rev. Food Sci. Food Saf.* **2021**, *20*, 5765–5801. [CrossRef]
41. Lu, B.; Han, F.; Aheto, J.H.; Rashed, M.M.A.; Pan, Z. Artificial bionic taste sensors coupled with chemometrics for rapid detection of beef adulteration. *Food Sci. Nutr.* **2021**, *9*, 5220–5228. [CrossRef]
42. Huang, K.; Ning, H.; Hu, N.; Liu, F.; Wu, X.; Wang, S.; Liu, Y.; Zou, R.; Yuan, W.; Wu, L. Ultrasensitive MWCNT/PDMS composite strain sensor fabricated by laser ablation process. *Compos. Sci. Technol.* **2020**, *192*, 108105. [CrossRef]
43. Li, D.; Wang, Z.; Liang, Z.; Zhu, F.; Xu, T.; Cui, X.; Zhao, P. Analyzing rice grain collision behavior and monitoring mathematical model development for grain loss sensors. *Agriculture* **2022**, *12*, 839. [CrossRef]
44. Niu, X.; Jia, W.; Qian, S.; Zhu, J.; Zhang, J.; Hou, X.; Mu, J.; Geng, W.; Cho, J.; He, J.; et al. High-performance PZT-based stretchable piezoelectric nanogenerator. *ACS Sustain. Chem. Eng.* **2019**, *7*, 979–985. [CrossRef]
45. Hassani, S.; Dackermann, U. A systematic review of advanced sensor technologies for non-destructive testing and structural health monitoring. *Sensors* **2023**, *23*, 2204. [CrossRef]
46. Ou, M.; Hu, T.; Hu, M.; Yang, S.; Jia, W.; Wang, M.; Jiang, L.; Wang, X.; Dong, X. Experiment of canopy leaf area density estimation method based on ultrasonic echo signal. *Agriculture* **2022**, *12*, 1569. [CrossRef]
47. Yin, L.; Jayan, H.; Cai, J.; El-Seedi, H.R.; Guo, Z.; Zou, X. Spoilage monitoring and early warning for apples in storage using gas sensors and chemometrics. *Foods* **2023**, *12*, 2968. [CrossRef]
48. Gao, S.; Zhou, R.; Zhang, D.; Zheng, X.; El-Seedi, H.R.; Chen, S.; Niu, L.; Li, X.; Guo, Z.; Zou, X. Magnetic nanoparticle-based immunosensors and aptasensors for mycotoxin detection in foodstuffs: An update. *Compr. Rev. Food Sci. Food Saf.* **2024**, *23*, e13266. [CrossRef]
49. Han, Z.; Ahmad, W.; Rong, Y.; Chen, X.; Zhao, S.; Yu, J.; Zheng, P.; Huang, C.; Li, H. A gas sensors detection system for real-time monitoring of changes in volatile organic compounds during oolong tea processing. *Foods* **2024**, *13*, 1721. [CrossRef]
50. Wang, M.; Zhang, A.; Pan, H.; Liu, F.; Chang, P.; Wang, J.; Lin, R.; Wang, B. Highly sensitive optical fiber temperature sensor based on microwave photonic filter with enhanced Vernier effect. *IEEE Sens. J.* **2024**, *24*, 6213–6218. [CrossRef]
51. Kumar, R.; Mandal, N. SAW sensor basics on material, antenna, and applications: A review. *IEEE Sens. J.* **2024**, *24*, 5713–5731. [CrossRef]
52. Zhang, G.; Li, P.; Wang, X.; Xia, Y.; Yang, J. Flexible battery-free wireless sensor array based on functional gradient-structured wood for pressure and temperature monitoring. *Adv. Funct. Mater.* **2023**, *33*, 2208900. [CrossRef]
53. Wang, F.; Chen, L.; Wang, Q.; Qin, W.; Meng, Z.; Yin, Y. Design and experimental validation of a flow-guided weighing-based grain mass flow sensor for wheat combine harvester. *Comput. Electron. Agric.* **2026**, *240*, 111224. [CrossRef]
54. Han, F.; Huang, X.; Mahunu, G.K. Exploratory review on safety of edible raw fish per the hazard factors and their detection methods. *Trends Food Sci. Technol.* **2017**, *59*, 37–48. [CrossRef]
55. Wang, F.; Zhu, Y.; Qian, L.; Yin, Y.; Yuan, Z.; Dai, Y.; Zhang, T.; Yang, D.; Qiu, F. Lamellar Ti_3C_2 MXene composite decorated with platinum-doped MoS_2 nanosheets as electrochemical sensing functional platform for highly sensitive analysis of organophosphorus pesticides. *Food Chem.* **2024**, *459*, 140379. [CrossRef] [PubMed]
56. Shoaib, M.; Li, H.; Khan, I.M.; Hassan, M.; Zareef, M.; Niazi, S.; Chen, Q. Emerging MXenes-based aptasensors: A paradigm shift in food safety detection. *Trends Food Sci. Technol.* **2024**, *151*, 104635. [CrossRef]
57. Marimuthu, M.; Xu, K.; Song, W.; Chen, Q.; Wen, H. Safeguarding food safety: Nanomaterials-based fluorescent sensors for pesticide tracing. *Food Chem.* **2025**, *463*, 141288. [CrossRef]
58. Dong, X.; Huang, A.; He, L.; Cai, C.; You, T. Recent advances in foodborne pathogen detection using photoelectrochemical biosensors: From photoactive material to sensing strategy. *Front. Sustain. Food Syst.* **2024**, *8*, 1432555. [CrossRef]

59. Li, H.; Murugesan, A.; Shoaib, M.; Sheng, W.; Chen, Q. Functionalized metal-organic frameworks with biomolecules for sensing and detection applications of food contaminants. *Crit. Rev. Food Sci. Nutr.* **2025**, *65*, 5218–5250. [CrossRef]
60. Zhang, L.; Chen, M.; Duan, H.; Bu, Q.; Dong, X. Recent advances of optical sensors for point-of-care detection of phthalic acid esters. *Front. Sustain. Food Syst.* **2024**, *8*, 1474831. [CrossRef]
61. Gao, S.; Yang, W.; Zheng, X.; Wang, T.; Zhang, D.; Zou, X. Advances of nanobody-based immunosensors for detecting food contaminants. *Trends Food Sci. Technol.* **2025**, *156*, 104871. [CrossRef]
62. Qu, L.; Zhang, X.; Chu, Y.; Zhang, Y.; Lin, Z.; Kong, F.; Ni, X.; Zhao, Y.; Lu, Q.; Zou, B. Research progress on nanotechnology-driven enzyme biosensors for electrochemical detection of biological pollution and food contaminants. *Foods* **2025**, *14*, 1254. [CrossRef]
63. Vera, J.; Conejero, W.; Mira-Garcia, A.B.; Mira-Garcia, A.B.; Conesa, M.R.; Ruiz-Sánchez, M.C. Towards irrigation automation based on dielectric soil sensors. *J. Hortic. Sci. Biotechnol.* **2021**, *96*, 696–707. [CrossRef]
64. Mochen, L.; Kuankuan, Y.; Yinfa, Y.; Zhanhua, S.; Fuyang, T.; Fade, L.; Yao, L. Multi-spectral evaluation of total nitrogen, phosphorus and potassium content in soil using Vis-NIR spectroscopy based on a modified support vector machine with whale optimization algorithm. *Soil Tillage Res.* **2025**, *252*, 106567. [CrossRef]
65. White, R.M.; Voltmer, F.W. Direct piezoelectric coupling to surface elastic waves. *Appl. Phys. Lett.* **1965**, *7*, 314–316. [CrossRef]
66. Coquin, G.A.; Tiersten, H.F. Analysis of the excitation and detection of piezoelectric surface waves in quartz by means of surface electrodes. *J. Acoust. Soc. Am.* **1967**, *41*, 921–939. [CrossRef]
67. Hassan, M.; Xu, Y.; Sayada, J.; Zareef, M.; Jiao, T.; Chen, M.; Chen, X.; Li, H.; Chen, Q. Trends in smart surface-enhanced Raman scattering sensors for food hazards. *Trends Food Sci. Technol.* **2025**, *163*, 105199. [CrossRef]
68. Gao, S.; Sun, Q.; Katona, J.; Zhang, D.; Zhang, Y.; Zou, X. Recent advances in metal-organic framework nanozyme (MOFzyme)-based biosensors for detecting food contaminants. *J. Agric. Food Chem.* **2025**, *73*, 23045–23077. [CrossRef]
69. Ingebrigtsen, K.A. Surface waves in piezoelectrics. *J. Appl. Phys.* **1969**, *40*, 2681–2686. [CrossRef]
70. Campbell, C. *Surface Acoustic Wave Devices for Mobile and Wireless Communications*; Academic Press: San Diego, CA, USA, 1998.
71. Morgan, D.P. *Surface Acoustic Wave Filters: With Applications to Electronic Communications and Signal Processing*, 2nd ed.; Academic Press: Oxford, UK, 2007.
72. Laurent, T.; Bastien, F. Lamb and shear-horizontal wave production by interdigital transducers deposited on both sides of a piezoelectric plate. *J. Acoust. Soc. Am.* **1996**, *99*, 2876–2882. [CrossRef]
73. Zhang, N.; Guo, X.; Chen, G. IDT-TAM integrated model for IT adoption. *Tsinghua Sci. Technol.* **2008**, *13*, 306–311. [CrossRef]
74. Gao, H.; Liu, Y.; Li, G.; Liu, H.; Shang, Y.; Ma, Z. On-demand design of terahertz metasurface sensors for detecting plant endogenous and exogenous molecules. *Agriculture* **2025**, *15*, 1481. [CrossRef]
75. Wu, X.; Yuan, Z.; Gao, S.; Zhang, X.; El-Mesery, H.S.; Lu, W.; Dai, X.; Xu, R. Nanostructure-engineered optical and electrochemical biosensing toward food safety assurance. *Foods* **2025**, *14*, 3021. [CrossRef]
76. Jayan, H.; Zhou, R.; Sun, C.; Wang, C.; Yin, L.; Zou, X.; Guo, Z. Intelligent gas sensors for food safety and quality monitoring: Advances, applications, and future directions. *Foods* **2025**, *14*, 2706. [CrossRef]
77. Huang, X.; Qi, Y.; Li, Z.; Zhang, N.; Qin, Z.; Du, L.; Shi, J.; Zou, X. Development strategies and applications of cell-based electrochemical taste sensors. *J. Food Meas. Charact.* **2025**, *19*, 8116–8131. [CrossRef]
78. Du, X.; Huang, J.S.; Shi, Q.; Li, T.; Wang, Y.; Liu, H.; Zhang, Z.; Yu, N.; Yang, N. A remote strawberry health monitoring system performed with multiple sensors approach. *Agriculture* **2025**, *15*, 1690. [CrossRef]
79. Gao, S.; Zheng, X. Innovative applications of Au-Ag bimetallic nanoparticles in food safety: Detection of bacterial pathogens and mycotoxins through advanced biosensing technologies. *J. Food Compos. Anal.* **2025**, *148*, 108518. [CrossRef]
80. Giurgiutiu, V. Tuned Lamb wave excitation and detection with piezoelectric wafer active sensors for structural health monitoring. *J. Intell. Mater. Syst. Struct.* **2005**, *16*, 291–305. [CrossRef]
81. Jin, J.; Quek, S.T.; Wang, Q. Design of interdigital transducers for crack detection in plates. *Ultrasonics* **2005**, *43*, 481–493. [CrossRef]
82. Xu, B.; Giurgiutiu, V. Single mode tuning effects on Lamb wave time reversal with piezoelectric wafer active sensors for structural health monitoring. *J. Nondestruct. Eval.* **2007**, *26*, 123–134. [CrossRef]
83. Zhou, R.; Ye, W.; Ma, L.; Qiu, G.; Zhang, Y.; Gao, S.; Wang, Y.; Guo, Z.; Zou, X. Advances in flexible surface-enhanced Raman scattering sensors for foodborne pathogen detection. *Food Qual. Saf.* **2025**, *9*, fyaf047. [CrossRef]
84. Huang, X.W.; Li, Z.H.; Zou, X.B.; Shi, J.Y.; Mao, H.P.; Zhao, J.W.; Hao, L.M.; Mel, H. Detection of meat-borne trimethylamine based on nanoporous colorimetric sensor arrays. *Food Chem.* **2016**, *197*, 930–936. [CrossRef]
85. Chen, Q.; Hu, W.; Su, J.; Li, H.; Ouyang, Q.; Zhao, J. Nondestructively sensing of total viable count (TVC) in chicken using an artificial olfaction system based colorimetric sensor array. *J. Food Eng.* **2016**, *168*, 259–266. [CrossRef]
86. Li, H.; Kutsanedzie, F.; Zhao, J.; Chen, Q. Quantifying total viable count in pork meat using combined hyperspectral imaging and artificial olfaction techniques. *Food Anal. Methods* **2016**, *9*, 3015–3024. [CrossRef]
87. Lanza di Scalea, F.; Bartoli, I. Temperature effects in ultrasonic Lamb wave structural health monitoring systems. *J. Acoust. Soc. Am.* **2008**, *124*, 161–174. [CrossRef]

88. Yu, L.; Giurgiutiu, V. In Situ 2-D piezoelectric wafer active sensors arrays for guided wave damage detection. *Ultrasonics* **2008**, *48*, 117–134. [CrossRef]
89. Salas, K.I.; Cesnik, C.E.S. Guided wave excitation by a CLoVER transducer for structural health monitoring: Theory and experiments. *Smart Mater. Struct.* **2009**, *18*, 075005. [CrossRef]
90. Lanza di Scalea, F.; Matt, H.; Bartoli, I.; Coccia, S.; Park, G.; Farrar, C. Health monitoring of UAV wing skin-to-spar joints using guided waves and macro fiber composite transducers. *J. Intell. Mater. Syst. Struct.* **2007**, *18*, 373–388. [CrossRef]
91. Mańka, M.; Martowicz, A.; Rosiek, M.; Stepinski, T.; Uhl, T. Tunable interdigital transducers made of piezoelectric macro-fiber composite. *Smart Mater. Struct.* **2016**, *25*, 115022. [CrossRef]
92. Moutaouekkil, M.; Streque, J.; Marbouh, O.; El Boudouti, E.H.; Elmazria, O.; Pernod, P.; Bou Matar, O.; Talbi, A. Contribution of ribbon-structured SiO_2 films to AlN-based and AlN/diamond-based Lamb wave resonators. *Sensors* **2023**, *23*, 6284. [CrossRef]
93. Jiang, Y.; Jing, X.; Li, J.; Zeng, X.; Pelenovich, V.; Xu, C.; Xiong, Z.; Zhang, J.; Yang, B. Extreme high temperature tolerant AlN thin film ultrasonic transducer and its application for bolt preload measurement. *J. Alloys Compd.* **2025**, *1027*, 180498. [CrossRef]
94. Liang, C.; Yan, C.; Zhai, S.; Wang, Y.; Hu, A.; Wang, W.; Pan, Y. Recent progress in flexible surface acoustic wave sensing technologies. *Micromachines* **2024**, *15*, 357. [CrossRef]
95. Bar-Cohen, Y.; Anderson, I.A. Electroactive polymer actuators-background review. *Mech. Soft Mater.* **2019**, *1*, 5. [CrossRef]
96. Wang, R.; Bhave, S.A.; Bhattacharjee, K. Design and fabrication of S0 Lamb-wave thin-film lithium niobate micromechanical resonators. *J. Microelectromech. Syst.* **2015**, *24*, 300–308. [CrossRef]
97. Mohammadgholiha, M.; Moll, J.; Tschöke, K.; Kruska, C.; Gebhardt, S.E.; De Marchi, L. Unidirectional frequency-steerable acoustic transducer for guided ultrasonic wave damage imaging. *Mech. Syst. Signal Process.* **2025**, *229*, 112505. [CrossRef]
98. Tong, X.; Zou, Y.; Wen, Z.; Liu, Z.; Luo, T.; Zhou, J.; Liu, H.; Ren, Y.; Xu, Q.; Liu, W.; et al. 6 GHz Lamb wave acoustic filters based on A1-mode lithium niobate thin film resonators with checker-shaped electrodes. *Microsyst. Nanoeng.* **2024**, *10*, 130. [CrossRef]
99. Dangi, A.; Liu, T.; Kim, J.N.; Kothapalli, S.-R.; Choi, K.; Trolier-McKinstry, S.; Jackson, T. Flexible thin-film PZT ultrasonic transducers on polyimide substrates. *Sensors* **2021**, *21*, 1014. [CrossRef]
100. Zhao, T.; Li, J.; Yang, X.; Yin, Z. A review of the preparation and application of lead zirconate titanate (PZT) thin film sensors. *J. Mater. Chem. C* **2025**, *13*, 15807–15851. [CrossRef]
101. Zhai, X.; Li, Z.; Zhang, J.; Shi, J.; Zou, X.; Huang, X.; Zhang, D.; Sun, Y.; Yang, Z.; Holmes, M.; et al. Natural biomaterial-based edible and pH-sensitive films combined with electrochemical writing for intelligent food packaging. *J. Agric. Food Chem.* **2018**, *66*, 12836–12846. [CrossRef]
102. Zhou, J.-W.; Zou, X.-M.; Song, S.-H.; Chen, G.-H. Quantum dots applied to methodology on detection of pesticide and veterinary drug residues. *J. Agric. Food Chem.* **2018**, *66*, 1307–1319. [CrossRef]
103. Zhu, X.; Chikangaise, P.; Shi, W.; Chen, W.-H.; Yuan, S. Review of intelligent sprinkler irrigation technologies for remote autonomous system. *Int. J. Agric. Biol. Eng.* **2018**, *11*, 23. [CrossRef]
104. Li, Y.; Luo, S.; Sun, L.; Kong, D.; Sheng, J.; Wang, K.; Dong, C. A green, simple, and rapid detection for amaranth in candy samples based on the fluorescence quenching of nitrogen-doped graphene quantum dots. *Food Anal. Methods* **2019**, *12*, 1658–1665. [CrossRef]
105. Acosta, M.; Novak, N.; Rojas, V.; Patel, S.; Vaish, R.; Koruza, J.; Rossetti, G.A.; Rödel, J. $BaTiO_3$-based piezoelectrics: Fundamentals, current status, and perspectives. *Appl. Phys. Rev.* **2017**, *4*, 041305. [CrossRef]
106. Saito, Y.; Takao, H.; Tani, T.; Nonoyama, T.; Takatori, K.; Homma, T.; Nagaya, T.; Nakamura, M. Lead-free piezoceramics. *Nature* **2004**, *432*, 84–87. [CrossRef]
107. Lin, H.; Xu, P.T.; Sun, L.; Bi, X.K.; Zhao, J.W.; Cai, J.R. Identification of eggshell crack using multiple vibration sensors and correlative information analysis. *J. Food Process Eng.* **2018**, *41*, e12894. [CrossRef]
108. Bonah, E.; Huang, X.; Yi, R.; Aheto, J.H.; Osae, R.; Golly, M. Electronic nose classification differentiation of bacterial foodborne pathogens based on support vector machine optimized with particle swarm optimization algorithm. *J. Food Process Eng.* **2019**, *42*, e13236. [CrossRef]
109. Wang, X.; Wu, J.; Xiao, D.; Zhu, J.; Cheng, X.; Zheng, T.; Zhang, B.; Lou, X.; Wang, X. Giant piezoelectricity in potassium-sodium niobate lead-free ceramics. *J. Am. Chem. Soc.* **2014**, *136*, 2905–2910. [CrossRef]
110. Takenaka, T.; Nagata, H. $(Bi_{1/2}Na_{1/2})TiO_3$-$BaTiO_3$ system for lead-free piezoelectric ceramics. *Jpn. J. Appl. Phys.* **1991**, *30*, 2236–2239. [CrossRef]
111. Reichmann, K.; Feteira, A.; Li, M. Bismuth sodium titanate based materials for piezoelectric actuators. *Materials* **2015**, *8*, 8467–8495. [CrossRef]
112. Cui, L.; Xue, X.; Le, F.; Mao, H.; Ding, S. Design and experiment of electro hydraulic active suspension for controlling the rolling motion of spray boom. *Int. J. Agric. Biol. Eng.* **2019**, *12*, 72–81. [CrossRef]
113. Li, L.; Xie, S.; Ning, J.; Chen, Q.; Zhang, Z. Evaluating green tea quality based on multisensor data fusion combining hyperspectral imaging and olfactory visualization systems. *J. Sci. Food Agric.* **2019**, *99*, 1787–1794. [CrossRef]

114. Lin, H.; Yan, S.; Song, B.; Wang, Z.; Sun, L. Discrimination of aged rice using colorimetric sensor array combined with volatile organic compounds. *J. Food Process Eng.* **2019**, *42*, e13037. [CrossRef]
115. Dai, C.; Huang, X.; Huang, D.; Lv, R.; Sun, J.; Zhang, Z.; Aheto, J.H. Real-time detection of saponin content during the fermentation process of Tremella aurantialba using a homemade artificial olfaction system. *J. Food Process Eng.* **2019**, *42*, e13101. [CrossRef]
116. Haider, S.T.; Shah, M.A.; Lee, D.G.; Hur, S. A review of the recent applications of aluminum nitride-based piezoelectric devices. *IEEE Access* **2023**, *11*, 58779–58795. [CrossRef]
117. Lu, R.; Yang, Y.; Link, S.; Gong, S. A1 resonators in 128° Y-cut lithium niobate with electromechanical coupling of 46.4%. *J. Microelectromech. Syst.* **2020**, *29*, 313–319. [CrossRef]
118. Stepinski, T.; Mańka, M.; Martowicz, A. Interdigital Lamb wave transducers for applications in structural health monitoring. *NDT E Int.* **2017**, *86*, 199–210. [CrossRef]
119. Mańka, M.; Rosiek, M.; Martowicz, A.; Stepinski, T.; Uhl, T. PZT based tunable interdigital transducer for Lamb waves based NDT and SHM. *Mech. Syst. Signal Process.* **2016**, *78*, 71–83. [CrossRef]
120. Trolier-McKinstry, S.; Muralt, P. Thin film piezoelectrics for MEMS. *J. Electroceram.* **2004**, *12*, 7–17. [CrossRef]
121. Muralt, P. Ferroelectric thin films for micro-sensors and actuators: A review. *J. Micromech. Microeng.* **2000**, *10*, 136–146. [CrossRef]
122. Setter, N.; Damjanovic, D.; Eng, L.; Fox, G.; Gevorgian, S.; Hong, S.; Kingon, A.; Kohlstedt, H.; Park, N.Y.; Stephenson, G.B.; et al. Ferroelectric thin films: Review of materials, properties, and applications. *J. Appl. Phys.* **2006**, *100*, 051606. [CrossRef]
123. Muralt, P.; Ledermann, N.; Baborowski, J.; Barzegar, A.; Gentil, S.; Belgacem, B.; Petitgrand, S.; Bosseboeuf, A.; Setter, N. Piezoelectric micromachined ultrasonic transducers based on PZT thin films. *IEEE Trans. Ultrason. Ferroelectr. Freq. Control* **2005**, *52*, 2276–2288. [CrossRef]
124. Lin, C.M.; Yantchev, V.; Zou, J.; Chen, Y.Y.; Pisano, A.P. Micromachined one-port aluminum nitride Lamb wave resonators utilizing the lowest-order symmetric mode. *J. Microelectromech. Syst.* **2014**, *23*, 78–91. [CrossRef]
125. Hou, R.; Hutson, D.; Kirk, K.J.; Fu, Y.Q. AlN thin film transducers for high temperature non-destructive testing applications. *J. Appl. Phys.* **2012**, *111*, 074510. [CrossRef]
126. Yantchev, V.; Katardjiev, I. Thin film Lamb wave resonators in frequency control and sensing applications: A review. *J. Micromech. Microeng.* **2013**, *23*, 043001. [CrossRef]
127. Lam, C.S.; Zou, J.; Lin, C.M.; Pisano, A.P. Transducer design for AlN Lamb wave resonators. *J. Appl. Phys.* **2017**, *121*, 154502. [CrossRef]
128. Zou, J.; Gao, A.; Lin, C.M.; Pisano, A.P. The multi-mode resonance in AlN Lamb wave resonators. *J. Microelectromech. Syst.* **2018**, *27*, 973–984. [CrossRef]
129. Zou, J.; Gao, A.; Pisano, A.P. Ultralow acoustic loss micromachined butterfly Lamb wave resonators on AlN plates. *IEEE Trans. Ultrason. Ferroelectr. Freq. Control* **2020**, *67*, 671–679. [CrossRef]
130. Zou, J.; Gao, A.; Pisano, A.P. Spectrum-clean S1 AlN Lamb wave resonator with damped edge reflectors. *Appl. Phys. Lett.* **2020**, *116*, 023505. [CrossRef]
131. Sun, H.; Lv, S.; Zhang, A.; Song, C.; Sun, X.; Tan, F.; Liang, L.; Zhu, Y.; Zhao, J. High quality-factor and spectrum-clean AlN Lamb-wave resonators with optimized lateral reflection boundary conditions and transducer design. *Micromachines* **2022**, *13*, 779. [CrossRef]
132. Le, X.; Peng, L.; Pang, J.; Xu, Z.; Gao, C.; Xie, J. Humidity sensors based on AlN microcantilevers excited at high-order resonant modes and sensing layers of uniform graphene oxide. *Sens. Actuators B Chem.* **2019**, *283*, 198–206. [CrossRef]
133. Shao, S.; Luo, Z.; Wu, T. High figure-of-merit Lamb wave resonators based on Al0.7Sc0.3N thin film. *IEEE Electron Device Lett.* **2021**, *42*, 1378–1381. [CrossRef]
134. Esteves, G.; Young, T.R.; Tang, Z.; Yen, S.; Bauer, T.M.; Henry, M.D.; Olsson, R.H. Al0.68Sc0.32N Lamb wave resonators with electromechanical coupling coefficients near 10.28%. *Appl. Phys. Lett.* **2021**, *118*, 171902. [CrossRef]
135. Kawai, H. The piezoelectricity of poly(vinylidene fluoride). *Jpn. J. Appl. Phys.* **1969**, *8*, 975–976. [CrossRef]
136. Lovinger, A.J. Ferroelectric polymers. *Science* **1983**, *220*, 1115–1121. [CrossRef]
137. Martins, P.; Lopes, A.C.; Lanceros-Mendez, S. Electroactive phases of poly(vinylidene fluoride): Determination, processing and applications. *Prog. Polym. Sci.* **2014**, *39*, 683–706. [CrossRef]
138. Ribeiro, C.; Costa, C.M.; Correia, D.M.; Nunes-Pereira, J.; Oliveira, J.; Martins, P.; Gonçalves, R.; Cardoso, V.F.; Lanceros-Méndez, S. Electroactive poly(vinylidene fluoride)-based structures for advanced applications. *Nat. Protoc.* **2018**, *13*, 681–704. [CrossRef]
139. Guzman, E.; Cugnoni, J.; Gmür, T.; Bonhôte, P.; Schorderet, A. Survivability of integrated PVDF film sensors to accelerated ageing conditions in aeronautical/aerospace structures. *Smart Mater. Struct.* **2013**, *22*, 065020. [CrossRef]
140. Singh, R.K.; Lye, S.W.; Miao, J. PVDF nanofiber sensor for vibration measurement in a string. *Sensors* **2019**, *19*, 3739. [CrossRef]
141. Tian, W.; Zhang, J.; Yu, Y.; Wen, Z.; Song, J.; Pan, D.; Li, D.; Li, J.; Lee, S.; Jin, J.; et al. A broadband high-output acoustoelectric transducer based on electrospun BTO/PVDF-HFP nanofiber. *ACS Appl. Energy Mater.* **2026**, *9*, 6930–6943. [CrossRef]
142. Bent, A.A.; Hagood, N.W. Piezoelectric fiber composites with interdigitated electrodes. *J. Intell. Mater. Syst. Struct.* **1997**, *8*, 903–919. [CrossRef]

143. Wilkie, W.K.; Inman, D.J.; Lloyd, J.M.; High, J.W. Anisotropic laminar piezocomposite actuator incorporating machined PMN-PT single-crystal fibers. *J. Intell. Mater. Syst. Struct.* **2006**, *17*, 15–28. [CrossRef]
144. Birchmeier, M.; Gsell, D.; Juon, M.; Brunner, A.J.; Paradies, R.; Dual, J. Active fiber composites for the generation of Lamb waves. *Ultrasonics* **2009**, *49*, 73–82. [CrossRef]
145. Brunner, A.J.; Birchmeier, M.; Melnykowycz, M.M.; Barbezat, M. Piezoelectric fiber composites as sensor elements for structural health monitoring and adaptive material systems. *J. Intell. Mater. Syst. Struct.* **2009**, *20*, 1045–1055. [CrossRef]
146. Collet, M.; Ruzzene, M.; Cunefare, K.A. Generation of Lamb waves through surface mounted macro-fiber composite transducers. *Smart Mater. Struct.* **2011**, *20*, 025020. [CrossRef]
147. Mańka, M.; Rosiek, M.; Martowicz, A.; Stepinski, T.; Uhl, T. Lamb wave transducers made of piezoelectric macro-fiber composite. *Struct. Control Health Monit.* **2013**, *20*, 1138–1158. [CrossRef]
148. Sun, Y.; Chen, J.; Li, X.; Lu, Y.; Zhang, S.; Cheng, Z. Flexible piezoelectric energy harvester/sensor with high voltage output over wide temperature range. *Nano Energy* **2019**, *61*, 337–345. [CrossRef]
149. Gorgin, R.; Luo, Y.; Wu, Z. Environmental and operational conditions effects on Lamb wave based structural health monitoring systems: A review. *Ultrasonics* **2020**, *105*, 106114. [CrossRef]
150. Le Traon, O.; Masson, S.; Chartier, C.; Janiaud, D. LGS and $GaPO_4$ piezoelectric crystals: New results. *Solid State Sci.* **2010**, *12*, 318–324. [CrossRef]
151. Pei, G.; Ma, B.; Zhang, Z.; Wang, C.; Deng, J.; Luo, J. High-temperature Pt-Al_2O_3 composite nano-thick interdigital electrodes for surface acoustic wave sensors. *Mater. Chem. Phys.* **2022**, *291*, 126697. [CrossRef]
152. Sui, W.; Feng, P.X.L. AlScN-on-SiC microelectromechanical Lamb wave resonators operating at high temperature up to 800 °C. *Appl. Phys. Lett.* **2024**, *125*, 022201. [CrossRef]
153. Streque, J.; Camus, J.; Laroche, T.; Hage-Ali, S.; M'JAhed, H.; Rammal, M.; Aubert, T.; Djouadi, M.A.; Ballandras, S.; Elmazria, O. Design and characterization of high-Q SAW resonators based on the AlN/sapphire structure intended for high-temperature wireless sensor applications. *IEEE Sens. J.* **2020**, *20*, 6985–6991. [CrossRef]
154. Zou, J.; Lin, C.M.; Chen, Y.Y.; Pisano, A.P. Theoretical study of thermally stable SiO_2/AlN/SiO_2 Lamb wave resonators at high temperatures. *J. Appl. Phys.* **2014**, *115*, 094510. [CrossRef]
155. Jin, H.; Zhou, J.; He, X.; Wang, W.; Guo, H.; Dong, S.; Wang, D.; Xu, Y.; Geng, J.; Luo, J.K.; et al. Flexible surface acoustic wave resonators built on disposable plastic film for electronics and lab-on-a-chip applications. *Sci. Rep.* **2013**, *3*, 2140. [CrossRef]
156. He, X.L.; Zhou, J.; Wang, W.B.; Xuan, W.P.; Yang, X.; Jin, H.; Luo, J.K. High performance dual-wave mode flexible surface acoustic wave resonators for UV light sensing. *J. Micromech. Microeng.* **2014**, *24*, 055014. [CrossRef]
157. Chen, J.; Wang, W.; Xuan, W.; Wang, X.; Dong, S.; Garner, S.; Cimo, P.; Luo, J. Flexible surface acoustic wave broadband strain sensors based on ultra-thin flexible glass substrate. *MRS Adv.* **2016**, *1*, 673–678. [CrossRef]
158. Wu, J.; Yin, C.; Zhou, J.; Li, H.; Liu, Y.; Shen, Y.; Garner, S.; Fu, Y.; Duan, H. Ultrathin glass-based flexible, transparent, and ultrasensitive surface acoustic wave humidity sensor with ZnO nanowires and graphene quantum dots. *ACS Appl. Mater. Interfaces* **2020**, *12*, 39817–39825. [CrossRef]
159. Zhou, J.; Guo, Y.; Wang, Y.; Ji, Z.; Zhang, Q.; Zhuo, F.; Luo, J.; Tao, R.; Xie, J.; Reboud, J.; et al. Flexible and wearable acoustic wave technologies. *Appl. Phys. Rev.* **2023**, *10*, 021311. [CrossRef]
160. Lamanna, L.; Piro, L.; Guido, F.; Rizzi, F.; De Vittorio, M. Recent progress in polymeric flexible surface acoustic wave devices. *Adv. Mater. Technol.* **2023**, *8*, 2300362. [CrossRef]
161. Pelrine, R.; Kornbluh, R.; Pei, Q.; Joseph, J. Electrostriction of polymer dielectrics with compliant electrodes as a means of actuation. *Sens. Actuators A Phys.* **1998**, *64*, 77–85. [CrossRef]
162. Pelrine, R.; Kornbluh, R.; Pei, Q.; Joseph, J. High-speed electrically actuated elastomers with strain greater than 100%. *Science* **2000**, *287*, 836–839. [CrossRef]
163. Carpi, F.; Chiarelli, P.; Mazzoldi, A.; De Rossi, D. Electromechanical characterisation of dielectric elastomer planar actuators: Comparative evaluation of different electrode materials and different counterloads. *Sens. Actuators A Phys.* **2003**, *107*, 85–95. [CrossRef]
164. Wissler, M.; Mazza, E. Electromechanical coupling in dielectric elastomer actuators. *Sens. Actuators A Phys.* **2007**, *138*, 384–393. [CrossRef]
165. Romasanta, L.J.; Lopez-Manchado, M.A.; Verdejo, R. Increasing the performance of dielectric elastomer actuators: A review from the materials perspective. *Prog. Polym. Sci.* **2015**, *51*, 188–211. [CrossRef]
166. Keplinger, C.; Sun, J.Y.; Foo, C.C.; Rothemund, P.; Whitesides, G.M.; Suo, Z. Stretchable, transparent, ionic conductors. *Science* **2013**, *341*, 984–987. [CrossRef]
167. Chortos, A.; Hajiesmaili, E.; Morales, J.; Clarke, D.R.; Lewis, J.A. 3D printing of interdigitated dielectric elastomer actuators. *Adv. Funct. Mater.* **2020**, *30*, 1907375. [CrossRef]
168. Wang, Z.; Cui, H.; Zhou, A.; Li, B.; Gorgin, R. Optimization design of an annular flexible IDT array based on a PDMS-PVDF substrate. *J. Intell. Mater. Syst. Struct.* **2023**, *34*, 2124–2132. [CrossRef]

169. Cui, H.; Wang, Z.; Zhang, J.; Fernández-López, A.; Güemes, A.; Gorgin, R. Optimization Design and Experimental Study for 2 Flexible Fan-shaped Interdigital Guided Wave Transducer. *Sens. Actuators A Phys.* **2024**, *376*, 115590. [CrossRef]
170. Wang, Z.; Qing, X.; Güemes, A.; Fernández-López, A.; Jiang, W. Design optimization and performance evaluation of a passive wireless SAW temperature sensor based on the GNU radio platform. *Smart Mater. Struct.* **2026**, *5*, ae6d5a. [CrossRef]